HHS Public Access

Author manuscript

Nature. Author manuscript; available in PMC 2022 December 01.

Reverse-translational identification of a cerebellar satiation network

Aloysius Y.T. Low[1], **Nitsan Goldstein**[1], **Jessica R. Gaunt**[2], **Kuei-Pin Huang**[3], **Norliyana Zainolabidin**[4], **Alaric K.K. Yip**[2], **Jamie R.E. Carty**[1], **Ju Y. Choi**[1], **Alekso M. Miller**[1], **Helen S.T. Ho**[4], **Clara Lenherr**[1,5], **Nicholas Baltar**[6], **Eiman Azim**[6], **October M. Sessions**[7], **Toh Hean Ch'ng**[2], **Amanda S. Bruce**[8], **Laura E. Martin**[9], **Mark A. Halko**[10], **Roscoe O. Brady Jr.**[11], **Laura M. Holsen**[12,13], **Amber L. Alhadeff**[3,14], **Albert I. Chen**[15,*], **J. Nicholas Betley**[1,14,*]

[1]Department of Biology, University of Pennsylvania, Philadelphia, PA 19104, USA

[2]LKC School of Medicine, Nanyang Technological University, Singapore 308232

[3]Monell Chemical Senses Center, Philadelphia, PA 19104, USA

[4]School of Biological Sciences, Nanyang Technological University, Singapore 308232

[5]Division of Neuroscience, King's College London, London WC2R 2LS United Kingdom

[6]Molecular Neurobiology Laboratory, Salk Institute, San Diego, CA 92037, USA

[7]School of Public Health, National University of Singapore, Singapore 117549

[8]Department of Pediatrics, University of Kansas Medical Center, Kansas City, KS 66160, USA

[9]Department of Population Health, University of Kansas Medical Center, Kansas City, KS 66160, USA

[10]McLean Hospital, Department of Psychiatry, Harvard University, Boston, MA 02478, USA

[11]Beth Israel Deaconess Medical Center, Harvard University, Boston, MA 02115, USA

[12]Division of Women's Health, Department of Medicine, Department of Psychiatry, Brigham and Women's Hospital, Boston, MA 02115, USA

[13]Harvard Medical School, Boston, MA 02115, USA

[14]Department of Neuroscience, University of Pennsylvania, Philadelphia, PA 19104, USA

[*]Correspondence: A.I. Chen (achen@scintillon.org) and J.N. Betley (jnbetley@sas.upenn.edu).

Author contributions

AYTL, AIC and JNB initiated the project and prepared the manuscript with comments from all authors. AYTL, NG, JRG, KPH, NZ, AKKY, JREC, JYC, AMM, HSTH, CL, LMH, ALA performed experiments. AYTL, NG, JG, EA, OMS, THC, ASB, LEM, MAH, ROB, LMH, ALA, IC and JNB designed experiments and analysed data.

Data and code availability

The sequencing datasets generated in this study are accessible at Gene Expression Omnibus under accession GSE184385. This manuscript contains all other datasets except the processed sequencing data, raw fibre photometry datasets and codes for analysis which have been uploaded to Mendeley Data. http://dx.doi.org/10.17632/d82xx5ybs2.1

Declaration of interest

The authors declare no competing interests.

Supplementary information

Supplementary Table 1. Details of statistics used and statistical results. Related to Fig. 1–4, and Extended Data Fig. 2–12.

[15]Scintillon Institute, San Diego, CA 92121, USA

Summary

The brain is the seat of body weight homeostasis. However, our inability to control the rising prevalence of obesity highlights a need to look beyond canonical feeding pathways to broaden our understanding of body weight control[1–3]. We used a reverse-translational approach to identify and anatomically, molecularly, and functionally characterise a neural ensemble that promotes satiation. Unbiased, task-based fMRI revealed striking differences in cerebellar responses to food in individuals with a genetic disorder characterized by insatiable appetite. Transcriptomic analyses in rodents revealed molecularly and topographically-distinct neurons in the anterior deep cerebellar nuclei (aDCN) that are activated by feeding or nutrient infusion in the gut. Selective activation of aDCN neurons dramatically decreased food intake by reducing meal size without compensatory changes to metabolic rate. We found that aDCN activity terminates food intake by elevating striatal dopamine levels and attenuating the phasic dopamine response to subsequent food consumption. Our study defines a conserved satiation centre that may represent a novel therapeutic target for the management of excessive eating, and underscores the utility of a "bedside-to-bench" approach for the identification of neural circuits that influence behaviour.

Introduction

Food intake is tightly regulated to ensure body weight homeostasis in the face of dynamic environmental challenges and food availability, as both starvation and overconsumption are evolutionarily unfavorable[2,4]. While it is appreciated that animals have redundant networks to ensure sufficient food intake[3], mechanisms also exist to limit food intake to maintain a stable body weight[1,5]. This delicate dance, referred to as "adaptive feeding," critically depends on interoceptive sensing of energy status, which weighs the motivation to eat with the need to avoid overconsumption. However, in an obesogenic environment this equilibrium is greatly skewed to favour positive energy balance[2]. Further, weight loss therapeutics that target known food intake-inhibitory mechanisms (e.g., hindbrain and hypothalamic circuits) are insufficient to maintain lasting weight loss[6]. This suggests the existence of yet-to-be-identified nodes that regulate food intake, and uncovering such mechanisms holds promise for the development of more effective obesity treatments.

How can we identify new circuits that inhibit food intake? We reasoned that individuals with the genetic disorder Prader-Willi syndrome (PWS), characterized by a lack of satiation and obesity[7], may have differences in neural activity in brain regions that control energy balance. Through this unbiased, reverse-translational approach, we identified the cerebellum as a surprisingly robust regulator of food intake. Our analysis of the cerebellar output structure has revealed the: 1) molecular and topographical logic of nutrient-sensitive neurons in the cerebellum, 2) pathways signalled via cerebellar output, and 3) behavioural and physiological mechanisms that terminate meals and control overall food intake. Our findings also highlight a powerful strategy for identifying and characterizing clinically-relevant neural circuits that underlie behaviour.

Results

Food cues activate the cerebellum

To identify brain regions that control food intake, we screened for dysregulated neural activity in individuals with PWS[8]. We analysed whole-brain fMRI blood-oxygen-level-dependent (BOLD) signals in response to food cues either while fasting or after eating (Extended Data Fig. 1). The deep cerebellum was the only brain region with significant differences in neural activity between individuals with PWS and control subjects (Fig. 1a, b) and our data suggest that a lack of cerebellar engagement in response to food cues may result in extreme hyperphagia.

We used rodent studies to determine the precise cerebellar region activated by food intake. RNA *in situ* hybridization analysis demonstrated that DCN neurons in the lateral (Lat) nucleus are activated by consumption of food (Fig. 1c–f). The post-ingestive, nutrient content of food is sufficient to activate Lat DCN neurons as Targeted Recombination in Active Population (TRAP) revealed activated neurons are enriched in the Lat DCN as well as in brain regions known to influence food intake (Extended Data Fig. 2)[3]. Together, these results demonstrate that hunger increases the responsiveness of the cerebellum to food cues and food in the human and mouse deep cerebellum, respectively.

Activation of aDCN reduces food intake

To determine the role of the cerebellum in regulating food intake, we manipulated DCN neuron activity and monitored consumption. We targeted viral-mediated expression of the excitatory designer chemogenetic receptor hM3D(Gq) to either the anterior DCN (aDCN which primarily includes Lat and Int subnuclei) or the posterior DCN (pDCN, which includes only the Int and Med subnuclei) (Extended Data Fig. 3a, e, g). Only activation of neurons in the Lat region of the aDCN (aDCN-LAT) reduced food intake (Fig. 2a–d, Extended Data Fig. 3b–i). aDCN-LAT activity led to a dramatic reduction in meal size and duration (satiation), but not frequency (satiety) or rate (Fig. 2e–g, Extended Data Fig. 4a–d), suggesting that aDCN-LAT neuron activity terminates meals. The food intake reduction is not state-dependent, as it occurs both when animals are food deprived and *ad libitum* fed (Extended Data Fig. 4e–h). Conversely, chemogenetic inhibition of aDCN-LAT neurons with hM4D(Gi) increased meal size (Fig. 2h), highlighting the physiological relevance of these neurons to satiation.

Many satiation signals serve as short-term inhibitors of food intake, and compensatory food intake or changes in energy expenditure render them ineffective for maintaining body weight changes[9]. The food intake reduction induced by DCN activation is not fully accounted for by changes in energy expenditure and we did not observe compensatory food intake in the subsequent 48 hours (Fig. 2i–l; Extended Data Fig. 4i–k). Furthermore, the food intake reduction is independent of the hedonic value of food as aDCN neural activity robustly inhibits intake of both chow and a high fat, high sugar diet (Fig. 2m; Extended Data Fig. 5).

Does the aDCN simply reduce intake or is it involved in the online calculation and adaptive control of calorie intake? We find that aDCN activity decreases food intake in a calorie-dependent manner, further supporting the notion that this region is specifically tuned to

energy status. When the caloric density of food was varied, animals with aDCN activation exhibited flexibility in the volume consumed to ingest the same number of total calories (Fig. 2n–p). Mice with aDCN activation increased consumption volume when the caloric density was decreased (Fig. 2o, p). Taken together, these results indicate that the activity in aDCN neurons diminishes food intake regardless of hunger state, palatability, or caloric density without compensatory changes in energy expenditure.

Identity of food-activated DCN neurons

Do DCN neurons that are activated by food have molecular or spatial distinctions? *In situ* hybridization histochemistry revealed that immediate-early gene expression is upregulated in glutamatergic neurons in the Lat nucleus of the DCN following refeeding (Extended Data Fig. 6). To define the molecular subtype identity of glutamatergic neurons, we profiled vGluT2-expressing transcriptomes in the DCN using single-nucleus RNA sequencing (snRNAseq)[10] (Extended Data Fig. 7a, b). We identified a graded and anti-correlated expression of two sets of genes (Fig. 3a; Extended Data Fig. 7c). This DCN expression pattern defines two classes of glutamatergic neurons: those that express *Spp1*, *Miat*, and *Crhr1* (class I) and those that express *Celf4*, *Dpp10* and *Uncd5* (class II) (Extended Data Fig. 7c–f). Multiplexed *in situ* hybridization analysis confirmed the nonoverlapping expression patterns and revealed a topography whereby class I neurons occupy the aDCN and class II neurons dominate the pDCN (Extended Data Fig. 7d–r). The activity-dependent expression of *Homer1a* is upregulated in class I but not class II DCN neurons in response to food intake (Fig. 3b–d; Extended Data Fig. 8a–s). Thus, our snRNAseq analysis uncovered a molecular signature that underlies the spatial organization and physiological responsivity of ‘food-activated’ glutamatergic neurons in the DCN.

To confirm that aDCN neurons are activated in response to food cues, we monitored the real-time calcium dynamics of class I aDCN neurons in awake behaving animals (Extended Data Fig. 8t–w). We find that there is a rapid and robust increase in neural activity of class I neurons upon food delivery in hungry but not sated animals (Fig. 3e, f; Extended Data Fig. 8x–cc). The onset of this activation is rapid and the responsiveness of these neurons is dependent on the interoceptive state of the animal, similar to the human studies (Fig. 1a, b). Based on the activity of class I aDCN neurons, we hypothesized that selectively activating these neurons will suppress food intake. Selective activation of class I glutamatergic neurons in the aDCN (where all glutamatergic neurons express Spp1) reduced food intake, similar to activation of the entire aDCN (Fig. 3g, h). The phenotype was specific for class I glutamatergic neurons in the aDCN-LAT, as activation of class II glutamatergic neurons in the aDCN-INT and pDCN did not change food intake (Fig. 3i, Extended Data Fig. 3g–i). Thus, class I glutamatergic neurons in the aDCN-LAT are an important node acting downstream of satiation signals, because these neurons are both activated by nutritive signals and capable of suppressing food intake.

DCN suppress food intake by reducing the phasic DA response to food

Both homeostatic (need-based, e.g., via hypothalamic nutrient-sensing neurons) and hedonic (reward-based, e.g., via dopamine circuitry) processes regulate feeding[3]. We next explored whether the cerebellum interacts with either homeostatic or hedonic networks that influence

food intake. The arcuate nucleus of the hypothalamus contains hunger-sensitive agouti-related protein (AgRP)-expressing neurons that drive food intake by interacting with downstream brain regions to regulate food intake[11]. We simultaneously activated both the aDCN-LAT and AgRP neurons in the arcuate nucleus and found that while acute activation of AgRP neurons in satiety robustly increases food intake, simultaneous activation of aDCN and AgRP neurons occluded the increase in food intake (Extended Data Fig. 9), demonstrating that aDCN neurons are capable of overriding hypothalamic control of food intake.

We next tested whether aDCN-LAT neuron activity suppresses food intake by modulating reward pathways[12]. Rewards (e.g., food) activate ventral tegmental area (VTA) dopamine (DA) neurons that release DA in the ventral striatum[13]. We monitored DA levels in the ventral striatum while activating aDCN neurons. Activating aDCN-LAT neurons led to sustained DA efflux that was not observed during aDCN-INT activation (Extended Data Fig. 10, 11). Importantly, we found a strong correlation between the levels of ventral striatal DA and the reduction in food intake following aDCN-LAT neuron activation (Extended Data Fig. 10j, 11n). This phenomenon was phenocopied by activation of VTA DA neurons, such that dose-dependent activation of VTA DA neurons (and therefore higher levels of striatal DA) led to greater reductions in food intake (Extended Data Fig. 12a–i). Thus, increased basal DA levels reduced the subsequent DA response to food (Extended Data Fig. 12j–m).

Does aDCN-LAT activity reduce food intake by increasing ventral striatal DA signalling? We selectively blocked the increase in striatal dopamine during ongoing aDCN-LAT neuron activation by inhibiting VTA-DA neurons. We first measured the ability of aDCN-LAT neuron activation to suppress feeding. Subsequently, in the same animals, we inhibited VTA-DA neurons and monitored DA levels in the ventral striatum (Fig. 4a, b, Extended Data Fig. 12n–q). The inhibition of VTA-DA neurons during aDCN-LAT stimulation restored DA levels to baseline (Fig. 4c, Extended Data Fig. 12r) without influencing motor behaviour (Extended Data Fig. 12s). Remarkably, blocking VTA-DA neuron activity during ongoing aDCN-LAT stimulation also completely restored food intake reductions caused by aDCN-LAT neuron activation alone (Fig. 4d). This rescue of food intake correlated with lower levels of striatal DA (Fig. 4e), suggesting that the ability of aDCN-LAT neurons to reduce food intake occurs via an increase in VTA-DA neuron activity.

DA response to food is increased by hunger and this response is critical to food intake[14]. But how is this phasic response influenced by ongoing aDCN-LAT activity? We find that aDCN-LAT activation leads to a reduction in the phasic DA transient that occurs in response to food (Fig. 4f–h). Restoring basal DA levels is sufficient to rescue the phasic DA burst (Fig. 4i, j). Taken together, these findings demonstrate that aDCN-LAT neurons reduce food intake by increasing basal DA levels in the ventral striatum that dampen the phasic DA response to food, likely reducing the reward value of additional food intake (Extended Data Fig. 13). This modulation of DA signalling provides a powerful means for cerebellar output pathways to adaptively regulate food intake, and provides a potential target for pharmacological or deep brain stimulation treatment of hyperphagia.

Discussion

The ability to regulate meal size is essential for maintaining body weight homeostasis. Thus, body weight regulation critically depends on interoceptive sensing of energy status and subsequent physiological signalling that balances the motivation for future food rewards with the need to avoid overconsumption. Here, we report the unexpected finding that cerebellar output neurons are activated by food cues to promote satiation and highlight the cerebellum as a potential therapeutic node for conditions such as obesity and Prader-Willi syndrome. Thus, cerebellar activity serves as a "brake" to reduce meal size and food intake.

Previous PWS imaging studies have revealed important insight into the neural substrates of hyperphagia[8,15] including aberrant activation in hypothalamic, limbic, prefrontal regions and the midbrain reward system. Our fMRI analysis adds to this literature by demonstrating a lack of food-anticipatory cerebellar activity in subjects with PWS. Perhaps, the cerebellum produces anticipatory responses to adaptively reduce food consumption before digestion is complete (Extended Data Fig. 13).

Anticipatory neural changes occur in neural circuits that respond to food intake[16,17] and these responses require gut-brain pathways that signal the detection of food[18]. We also demonstrate that the deep cerebellum is activated by nutrients detected in the gut. How might the cerebellum receive rapid satiation signals from the gut? We provide evidence that food images increase BOLD signal in the human cerebellum and that gut nutrients and consumption activates a select subset of neurons in the mouse cerebellum. The hindbrain, which receives direct vagal signals from the gut, has known projections to the cerebellum[19]. Thus, it is possible that vagal signalling through the hindbrain is a route by which nutrient information is transmitted to the cerebellum.

How does cerebellar output influence the networks that control food intake[20]? Our work demonstrates that cerebellar output dramatically increases striatal dopamine levels, leading to a reduction in the phasic dopamine response to food. The link between increased DA levels and reduced food intake may appear paradoxical, as larger dopamine signals are reinforcing, and depleting dopamine results in severe anorexia[21]. However, a long-lasting increase in baseline DA levels, similar to that observed during drug use[18], can result in a reduction in the phasic DA response to food[22]. This likely reduces meal size by decreasing the reward value of additional consumption. Importantly, dopamine signalling has known roles in hindbrain satiation networks that modulate food motivation based on interoceptive state[14,23]. Thus, modulation of the dopaminergic system is one key point of convergence for signals that regulate food intake[24] (Extended Data Fig. 13).

Methods

Neural response to food cues

Human Subjects—Subject characteristics have been previously reported[8]. Data were collected from individuals with Prader-Willi syndrome (PWS) [n=14; 12 F/2 M; 2 Type 1 Deletion, 8 Type 2 Deletion, 4 uniparental disomy; mean age (years)=24.3±11.3; mean BMI (kg/m^2) =32.1±7.8] and controls, individuals with simple obesity (OB group; n=14; 9 F/5 M;

mean age=25.0±10.3; mean BMI=32.4±3.5). Groups were matched on sex (Fisher's Exact Test significance=0.39), age (t(26)=0.18, non-significant (ns)), BMI (t(26)=0.14, ns), and handedness (all right-handed). Diagnosis of PWS was confirmed through chromosomal and DNA molecular analysis as previously described[25]. Concomitant psychotropic medications in the PWS group included (number of subjects): buspirone (1), clonazepam (1), divalproex (2), escitalopram (1), fluoxetine (1), fluvoxamine (1), lorazepam (1), quetiapine (1), risperidone (1), topiramate (1), sertraline (1), and ziprasidone (1). One PWS participant was being treated for hypothyroidism. Seven PWS subjects and all OB subjects were medication-free. All participants were free from current growth hormone treatment, history of appetite suppressant use, and history of neurological illness. This study was approved by the Human Subjects Committees at the University of Kansas (KUMC) and University of Rochester (URMC) Medical Centres. Written informed consent was obtained from parents and assent was obtained from participants.

Experimental protocol—Following a previously validated protocol[8,26–28], participants completed two scanning sessions varying in metabolic state; both sessions were completed on the same day and the order of sessions was counterbalanced across subjects. One session commenced after fasting for at least four hours (pre-meal: either prior to breakfast at 8:00 am or prior to lunch at 12:00 pm). The other session started within 15 minutes after eating a small 500-kcal meal standardized for microand macronutrient content (post-meal: either following breakfast at 8:30 am or following lunch at 12:30 pm) (Extended Data Fig. 1).

Food cue paradigm—During each scanning session, participants completed a food cue paradigm during which they passively viewed images of food, animals, and Gaussian-blurred low-level baseline control images. Visual stimuli of two categories (food and blurred baseline control) were obtained from LaBar and colleagues[29]. Stimuli of the animal (non-food) category were obtained from professional photographic sources and matched to food and blurred control images on brightness, resolution, and size. Unique sets of images were presented at pre- and post-meal sessions. The paradigm was programmed in NeuroSTIM (Neuroscan) and projected through 3D limited-view goggles (Resonance Technology, Inc.). A total of two 6.5-minute runs following a block design (2.5 sec/image + 0.5 sec interstimulus interval; 10 images/block; 13 blocks/run) were presented. Blocks of food and non-food categories alternated with blocks of blurred baseline control images, with order of category presentation counterbalanced across subjects. Prior to each run, participants were instructed to pay close attention to each image because they would be taking a memory test on the images immediately following the scanning session. During the recognition memory test, 50% of the images from the food and non-food categories were chosen for recall and interspersed with novel distracter images from the same category. Participants were instructed to press one key if they had seen the image in the scanner (old) and another if they had not seen the image (new).

MRI data acquisition—Collection of anatomical and functional MRI data was performed on a 3 Tesla Siemens Allegra or Trio scanner (Siemens, Erlangen, Germany). Participants' heads were immobilized with cushions. Most subjects (n=38) were scanned at KUMC on an Allegra scanner using a quadrature headcoil. The remaining subjects (n=5, all PWS) were

scanned on a Trio scanner using an 8-channel headcoil at URMC. At each scanning session (pre-meal and post-meal), one anatomical and two functional sequences were collected. T1-weighted anatomical images were acquired using similar 3D MP-RAGE sequences at each site [KUMC: coronal, repetition time/echo time (TR/TE)=23/4 ms, flip angle=8°, field of view (FOV)=256×192 mm, slice thickness=1 mm; URMC: sagittal, TR/TE=20/4 ms, flip angle=15°, FOV=256×256 mm, slice thickness=1 mm]. Single shot gradient echo planar imaging (EPI) fMRI scans were also acquired at each site using similar sequences (KUMC: 43 contiguous coronal slices, TR/TE=3000/40 ms, flip angle=90°, FOV=192×192 mm, slice thickness=3 mm, in-plane resolution=3×3 mm, 130 data points; URMC: 43 contiguous coronal slices, TR/TE=3000/36 ms, flip angle=90°, FOV=192×192 mm, slice thickness=3 mm, in-plane resolution=3×3 mm, 130 data points). A shorter TE (36 vs. 40 ms) at the URMC site provided ~7% higher signal-to-noise ratio (SNR) based on the typical T2* in cortical gray matter[30], but ~10% lower task-induced BOLD signal change. Because the fMRI contrast-to-noise ratio (CNR) is proportional to the product of SNR and BOLD signal changes, we estimated ~3% CNR at TE = 36 ms. Therefore, it was expected that the overall effect of the TE difference was not significant and within the range of the experimental variations. Moreover, given the rarity of PWS and the need for larger samples, the compromise of slightly different acquisitions was justified.

fMRI data analysis—fMRI results in a set of *a priori* regions of interest (ROIs) have been previously reported[8]. However, whole-brain results agnostic of *a priori* ROIs have not been described. fMRI data were pre-processed using Statistical Parametric Mapping (v12, SPM12; Wellcome Trust Centre for Neuroimaging) and custom routines in MATLAB (v_2016a Mathworks, Inc.). Volumes were realigned and corrected for bulk-head motion, normalized to the Montreal Neurological Institute (MNI) MNI152 brain template, and smoothed with a 6 mm Gaussian filter kernel and resampled at 3 mm isotropic. Next, outliers in the global mean image time series (threshold: 3.5 S.D.) and movement (threshold: 3.8mm translational movement or 0.05 radians rotational movement) were detected using an Artifact Detection Toolbox (http://www.nitrc.org/projects/artifact_detect/) and entered as nuisance regressors in the first-level general linear model.

Following pre-processing, first-level models were statistical analysis was performed at the single (first) level. SPM treats each voxel's BOLD time series according to a general linear model. Each epoch of trials was modelled using a boxcar function convolved with a canonical hemodynamic response function. The contrast of interest (food versus non-food) from the single-subject analysis was tested using linear contrasts, and SPM t-maps, then submitted to second-level random effects group analysis.

At the second (group) level, a full factorial ANOVA model was specified for the primary contrast of interest (food vs. non-food) to examine the *Group* (PWS, OB) x *Session* (pre-meal, post-meal) interaction at the whole-brain level. We report clusters that (a) were significant at $p<0.01$ uncorrected and (b) exceed an extent threshold of k=50. For clusters reaching statistical significance for the *Group* x *Session* interaction, parameter estimates were extracted with the REX toolbox[31] for analysis of simple effects in SPSS (version 24) and for visual display.

Mice—Adult C57BL/6J, *vGluT2*-IRES-Cre (Slc17a6tm2(cre)Lowl/J)[32], *DAT*-IRES-Cre (B6.SJLSlc6a$^{tm1.1(cre)}$Bkmn/J)[33], *TRAP2* (Fostm2.1(icre/ERT2)Luo/J)[34], *Ai9* (B6.Cg-Gt(*ROSA*)26Sortm9(CAG-tdTomato)Hze/J)[35], *vGluT2*-Cre (Tg(*Slc17a6*-icre)1Oki)[36], *Ai32* (B6.Cg-Gt(*ROSA*)26Sortm32$^{(CAG-COP4*H134R/EYFP)Hze}$/J)[35], *AgRP*-IRES-Cre (Agrp$^{tm1(cre)Lowl}$/J)[37], mice were 8–10 weeks old at the start of all experiments. Prior to experiments, mice were habituated for 2–3 days to experimental conditions such as handling, injections, bedding, chambers, attachment to patch-cords for fibre photometry and optogenetics, or attachment of gastric catheter infusion pumps. Littermates of the same sex were randomly assigned to experimental groups. Within-subject and between-subject statistical analyses were conducted on mice that have undergone all experimental conditions or were randomly assigned to experimental groups, respectively We did not observe significant sex differences between male and female mice in our experiments. Thus, both sexes were combined. All mice were housed in 19.56 cm x 30.91 cm x 13.34 cm (Thoren Caging Systems, Inc.; Model #9 Small mouse II Cage) at a maximum capacity of 5 mice of the same sex with animal bedding (The Andersons, Inc., Bed-o'Cobs laboratory animal bedding 1/8 inch) and nestlet (Ancare, NES3600-NESLETS) with free access to food (Altromin, #1324 – 10mm pellets) and water under a 12 hour light/dark cycle, under animal biosafety level 1 laboratory conditions, with controlled temperature of 21.5 to 22.3 degree Celsius, humidity 50±15%, and negative pressured rooms (−191.6 to 109.5 Pascal).

Eight-week old male mice were bred with either one or two females, and pups were weaned between postnatal day 21–28. Both sexes of all lines are viable and fertile. *vGluT2*::Cre mice were homozygous for Cre, *DAT*::Cre mice were heterozygous for Cre, and *AgRP*::Cre; *Ai32*, *TRAP2*; *Ai9*, double transgenic mice were heterozygous for each allele.

All procedures were approved by and conducted in accordance with the ethical guidelines of the Nanyang Technology University Singapore and the University of Pennsylvania Institutional Animal Care and Use Committee (NTU #151069, Penn #805793).

Recombinant Adeno-Associated Virus (rAAV) constructs—rAAV vectors:

AAV2-*hSyn*-hM3D(Gq)-mCherry (Addgene, LOT #v6236, CAT#50474-AAV2, 4.8×10^{13} GC/ml); AAV2-*hSyn*-DIO-hM3D(Gq)-mCherry (Addgene, LOT #v58216, CAT#44361-AAV2, 2.0×10^{13} GC/ml);

AAV2-*hSyn*-hM4D(Gi)-mCherry (Addgene, LOT#v54503, CAT#50475-AAV2, 2.1×10^{13} GC/ml); AAV2-Syn-FLEX-ultrasensitive protein calcium sensors (GCaMP6s)-WPRE-SV40 (Vigene, $1.35X10^{13}$ GC/ml, Addgene plasmid #100845 packaged);

AAV5-*hSyn*-DIO-hM4D(Gi)-mCherry (Addgene, LOT#v47232, CAT# 44362-AAV5, 1.3×10^{13} GC/ml);

AAV5-*hSyn*-DIO-hM3D(Gq)-mCherry (Addgene, LOT#v54404, CAT# 44361-AAV5, 1.3×10^{13} GC/ml);

AAV2-*hSyn*-mCherry (Addgene, LOT #v53550, CAT#114472-AAV2, 2.6×10^{13} GC/ml);

AAV2-*hSyn*-DIO-mCherry (Addgene, LOT #v54505, CAT#50459-AAV2, 1.8×10^{13} GC/ml);

AAV9-*hSyn*-DA4.2 (Vigene Biosciences, LOT #2018.07.02, CAT#hD01, 5.45×10^{13} GC/ml); and AAV9-*hSyn*-DA1h (Vigene Biosciences, LOT #2019.10.18, CAT#YL10010-AAV9, 2.04×10^{13} GC/ml).

Syn, human Synapsin 1 promoter. DIO, Double-floxed inverted orientation. hM4, human M4 muscarinic receptor. hM3, human M3 muscarinic receptor. GRABDA1h ($GRAB^{DA}$), GPCR activation-based DA sensor.

Viral injections and optic fibre implantation—Mice were anesthetized and viral injections and fibre implants were performed as previously described with modifications described below[18,38,39].

Bilateral injections of virus were performed to express either the excitatory designer receptor exclusively activated by designer drug (DREADD), hM3D(Gq) in the DCN (400 nl), aDCN (200 nl), pDCN (200 nl) or the VTA (200 nl) using the following coordinates: DCN: lambda −2.3 mm, midline ±1.35 mm, depth −2.5 mm; aDCN: lambda −2.05 mm, midline −2.1 mm, depth −2.4 mm; pDCN: lambda −2.36 mm, midline −1.25 mm, depth −2.3 mm; and VTA: bregma 3.2 mm, midline ±1.2 mm, and depth 4.4 mm, at a 10° angle from vertical in the lateral-medial direction.

For fibre photometry experiments, unilateral injections of a virus designed to express a fluorescent DA sensor[40] were performed in the ventral striatum (200 μl) following these coordinates: ventral striatum: bregma 0.98 mm, midline ±0.75, depth −4.05. Ferrule-capped optical fibre (400-mm core, NA 0.48, Doric, MF2.5, 400/430–0.48) was implanted 0.2 mm above the injection site and secured to the skull with three anchoring screws (stainless steel, 1.5 by 1.5 mm, #000–120 thread screws), Metabond cement (Parkell, S380) and dental cement (Lang Dental Manufacturing, Ortho-jet BCA Liquid, B1306 and Jet Tooth Shade Powder, 143069).

For optogenetics experiments, optical fibres (200 μm diameter core, NA 0.48) were implanted similarly as described above, using the following coordinates to target the ARC: bregma: −1.3 mm, midline 0.3 mm, depth −5.85 mm.

Food deprivation and restriction

Deprivation: Mice were caged with clean paper-based ALPHA-dri bedding (Shepherd Specialty Papers) to prevent mice from consuming corncob-based bedding and given *ad libitum* access to water during 24-hour food deprivation. Body weights were monitored to assure a 10–15% decrease from *ad libitum*-fed body weight prior to experiments. *Restriction:* To maintain 85–90% body weight during the conditioned place preference experiment, mice were weighed daily at the same time of day and given an aliquot of chow (~10% of body weight at 17:00). Mice were group housed, except for food restriction and TRAP experiments, in which mice were singly caged.

Open field assay

Mice were placed in a 450 (l) x 450 (b) X 400 (h) mm white walled acrylic arena, and movements were recorded for 10 minutes using a top view camera (Logitech c170 webcam). Video recordings of general locomotor activities were analysed with ANY-maze software (v_7.08 Stoelting). When repeated measures were required, a one-week interval was implemented, and flooring pattern was changed from plain white to green checkered pattern. Mice were returned to their homecages after each session.

Food intake experiments

Acute food intake—Mice were habituated for 1.5 h for two consecutive days to an empty cage with a water-resistant sheet of Kimtech bench-top-protector (#7546 Kimberly-Clark) as bedding, a material that enables convenient retrieval of chow crumbs for measurements. Mice received either CNO (1 mg/Kg) or vehicle (0.07% DMSO in 0.9% NaCl) injections 20 minutes before being placed in the cage. A 3-gram pellet of chow was provided and food intake was measured over a period of 1 hour by weighing the remaining food, accounting for crumbs.

Feeding microstructure for DCN neuron activation—*Ad libitum* fed hM3D(Gq)-expressing mice were habituated to feeding chamber for 1.5 hours for two consecutive days. Mice were either food deprived (24 hours) or *ad libitum* fed before feeding assessment. The experiment was designed in a counterbalanced manner. hM3D(Gq) mice were randomly separated into two groups, and received either CNO (1 mg/Kg) or vehicle injections 20 minutes before being placed in a 150 (l) x 85 (b) x 200 (h) mm transparent acrylic chamber for 1 hour with a 3-gram chow pellet attached to a corner with adhesive to prevent movement of chow pellet. Feeding behaviour was recorded using a video camera positioned to capture a clear view of the pellet. Remaining chow was measured to determine food intake and videos were analysed for feeding microstructures as previously described[41]. Bites on pellet was binned into 1 second, and defined as one bite. A bout is defined by bites that are discontinued for >5 seconds. A meal was considered terminated when an inter-bout-interval exceeded 5 minutes. Mice were refed and body weight was allowed to fully recover for 3 days before the counterbalance experiment was carried out. Experiments were conducted between 11:00 to 15:00 (light cycle). Feeding pattern was analysed using Graphic State (v_4).

12-hour food intake—Mice were individually caged and habituated to high fat high sugar diet (HFHS; C 1090 – 70 Obesity-inducing diet with 70% energy from fat) and to bedding made of a fine metal gauze (Stainless Steel Woven Wire Mesh) wrapped around c-fold towels for two days. This bedding absorbs urine to reduce food crumbs soaking up urine so that the weight of left-over food can be accurately measured. Mice were food deprived prior to the experiment in the behavioural apparatus and either CNO (1 mg/Kg) or vehicle was intraperitoneally injected 20 minutes before introducing approximately 8 g of either chow or HFHS, with *ad libitum* access to water. Food was measured at 30 minutes, 1 hour, 1.5 hours, 2 hours, 4 hours, 6 hours, 8 hours, 10 hours and 12 hours. Mice were injected with 1 mg/Kg CNO or vehicle every 2 hours for 12 hours. Experiments were conducted between 11:00 and 23:00.

Liquid diet intake—Mice were habituated to a home cage with a Kimtech bench-top-protector (#7546 Kimberly-Clark) flooring for 2 hours each day (2 days) with free access to liquid diets (Ensure®Original and Ensure®Plus) contained in custom-made 15 ml conical centrifuge tubes with drip-resistant metal sipper enabling accurate measurements of volume consumed. On the experimental day, mice were food deprived (24 hour) prior to the 1-hour liquid diet intake assay. CNO (1 mg/Kg) or vehicle was intraperitoneally injected 20 minutes before allowing access to the liquid diet. Experiments were conducted between 13:00 to 15:00.

Fibre photometry

Fibre photometry was performed and analysed as we have previously described[38,42,43]. 470 nm light at 211 Hz was used to excite $GRAB^{DA}$ and GCaMP. Additionally, an isosbestic 405 nm light at 566 Hz was used to control for artifacts caused by movement and bleaching in GCaMP recordings. Mice were habituated to the experimental procedures prior to recordings. DA sensing was conducted in a home cage without a cover. To avoid signal saturation, output power of 470 nm excitation light was adjusted to 50% (20 to 60 μW) and 405 nm excitation light was adjusted to 5% (2 to 10 μW) detection range of the photoreceiver. Power adjustments were done to compensate for variations in fibre placement and expression of DA1h and GCaMP so as to achieve similar baseline fluorescence signals across all mice. Before introducing stimuli (CNO/vehicle), 2–5 minutes of baseline DA1h and GCaMP fluorescence was measured and used for comparing post-stimulation signals. No water was provided during the recording session. Experiments were conducted between 11:00 and 17:00. Analysis was done using Synapse Tucker-Davis Technologies software.

Effects of food on DCN activity—Three weeks after surgery, mice were presented with either food or a non-food object (marble) while GCaMP fluorescence in glutamatergic DCN neurons was monitored. Mice were either food deprived for 24-h or fed *ad libitum* in a counterbalanced fashion prior to the start of recordings. Mice were attached to the fibre photometry systems. Following a two-minute baseline recording, a pellet of chow or a non-food object was presented to the animals in their cage. Within subjects comparisons were made. Mice were habituated to the non-food object for two days prior to recordings.

Effects of cerebellar and midbrain dopaminergic neuron activity on DA signalling—After two weeks of post-surgical recovery, mice with hM3D(Gq) expressed in the DCN or VTA and DA sensor expressed in the striatum were habituated to experimental procedures. CNO (0.025 to 2.5 mg/Kg) or vehicle was administered via i.p. injection to mice with hM3D(Gq) expression in the VTA, and 1 mg/Kg CNO or vehicle was injected to mice with DCN hM3D(Gq) expression after a 5-minute baseline recording. DA levels were recorded for 30 minutes after i.p. injection.

To determine the effects of VTA neuron activation on striatal dopamine signalling in response to food, mice with hM3D(Gq) expression in the VTA were food deprived (24 hours), and $GRAB^{DA}$ signal was monitored as described above. A pellet of chow was presented to the mice in their cage 15 minutes after i.p. injection of CNO (0.025 mg/Kg to 2.5 mg/Kg) or vehicle.

To study the effects of striatal dopamine signalling in response to food, mice with hM3D(Gq) expressed in the DCN, and mice with hM3D(Gq) expressed in the DCN and hM4D(Gi) expressed in VTA were 24-h food deprived. GRAB^{DA} signal was monitored as described above. After 20 minutes post CNO (1 mg/Kg) administration, a 10-minute baseline was recorded followed by a chow pellet presented to the mouse.

To investigate striatal dopamine signalling in response to food during aDCN-LAT activation and simultaneous aDCN-LAT activation and dopaminergic VTA inhibition, mice were 24-h food deprived and GRAB^{DA} signal was monitored as described above. A pellet of chow was presented to the mice in their cage 30 minutes after i.p. injection of CNO (1 mg/Kg).

Silencing VTA DA neurons during aDCN-LAT activation—Two weeks post-surgical recovery, mice with hM3D(Gq) expression in DCN were habituated to experimental procedures. During the following two weeks, open field (*ad libitum*) and 1 hour feeding assays (food deprived) were conducted. Vehicle and CNO administered experiments were 1 week apart for open field, and at least 3 days apart for feeding assays. This is to ensure novelty of open field apparatus, and for mice to recover in body weight. Mice undergo a second surgery to express hM4D(Gi) in VTA DA neurons, and GRAB^{DA} in the ventral striatum with a fibre implant for photometry recordings. Three weeks post-surgery, DA recordings, open field and 1 hour feeding assays were conducted with vehicle and CNO administration. Similar to open field, DA recording experiments were conducted 1 week apart.

Energy expenditure and activity

Mice fed with pellet chow (LabDiet Rodent 5001) were individually housed in training chambers for a 3-day acclimation and in recording chambers for a 1-day acclimation period prior to the data collection. Mice fed *ad libitum* received CNO (1 mg/Kg) 30 min before the onset of dark phase. Food intake, water intake, XYZ-axis movement, oxygen consumption, and carbon dioxide production were monitored by PhenoMaster for 2 days (TSE Systems Inc, MO). The chamber air was set in 0.3 L/min and was analysed for oxygen and carbon dioxide content every 30 min. Energy expenditure was calculated by Weir equation, 3.941 × oxygen consumption + 1.11 × carbon dioxide production[44].

Histology, immunohistochemistry, and imaging

Mice were deeply anesthetized with isoflurane (Clipper, 0010250) before being transcardially perfused with 1x phosphate-buffered saline (PBS, OmniPur, 6505) followed by 4% paraformaldehyde (4% PFA, MP Biomedicals, 150146). Brains were harvested and post-fixed in 4% PFA at 4°C for 2–6 hours then transferred to PBS. Coronal sections of 100–200μm were prepared in PBS with a vibrating blade microtome (Leica, VT1000 S). Free-floating brain sections were treated with washing buffer (0.1% TritonX100 (Sigma-Aldrich) in PBS) for 5 minutes three times and incubated in blocking buffer (1% BSA in 0.1% Triton X100 PBS) for 1 hour at room temperature[45]. Brain sections were then incubated for 12 h at 4°C in primary antibodies diluted in blocking buffer. Primary antibodies, guinea pig anti-tdTomato (1:20000)[11], guinea pig anti-vGluT2 (1:1000, Sigma-Aldrich, AB2251-I), rabbit anti-GFP (1:1000, # A-11122, Invitrogen), mouse anti-tyrosine

hydroxylase (1:500, Chemicon) and mouse anti-SMI 32 (1:1000, # SMI-32P, Biolegend) were used. Samples were washed with washing buffer for 5 minutes, repeated three times. Secondary antibodies Cy™3, Alexa Fluor®488 and Cy™5-conjugated donkey anti-guinea pig, -rabbit and -mouse (1:1000, Jackson ImmunoResearch), were diluted in blocking buffer with DAPI stain (1:500; D3571, Life technologies). Sections incubated for 2 hours at room temperature and were washed in PBS. Brain sections were mounted on a glass slide in mounting agent (Fluoro-Gel, 17985–10). To validate fibre position or virus reporter expression, images were collected on a stereo fluorescence microscope (Leica, M165FC). To quantify virally transduced cells expressing a reporter or colocalization studies, high magnification images were taken using an upright microscope (Leica DM6 with Leica TCS SPE scan head, and Leica EL6000 for external light source) with a 20x objective (0.80 NA). Images were taken in the linear range of the detector to avoid signal saturation. Images were analysed with NIH ImageJ (version 1.50g, and version 1.52a; NIH) and post-processed using Adobe Photoshop CS6.

Single-nucleus RNA sequencing

Tissue extraction and nuclei isolation—Mice were anesthetized and decapitated immediately. Brains were extracted and dissected in pre-chilled cutting solution (250 mM Sucrose, 26 mM $NaHCO_3$, 10 mM [D+] Glucose, 4 mM $MgCl_2$, 3 mM Myo-inositol, 2.5 mM KCl, 2 mM Sodium pyruvate, 1.25 mM NaH_2PO_42H2O, 0.5 mM Ascorbic acid, 0.1 mM $CaCl_2$, and 1 mM Kynurenic acid) and were sectioned using a vibratome (Leica VT-1200). The DCN was identified and micro-dissected from the cerebellar vibratome slices (Bregma −5.68 mm to −6.84 mm). Micro-dissected DCN were stored in chilled ACSF before homogenization.

Tissue was homogenized in a Dounce homogenizer with 2 ml homogenization buffer (0.25 M Sucrose, 25 mM KCl, 5 mM $MgCl_2$, 20 mM Tricine, pH 7.8), followed by addition of NP-40 (final concentration 0.3%) to lyse the cells. The suspension was filtered through a 40 μm filter (H13680–0040, Scienceware) to remove debris and multiplets. The 2 ml filtrate was mixed with 4.6 ml of 1.8 M Sucrose cushion buffer (1.8 M sucrose, 10mM Tris-HCl, 1.5 mM $MgCl_2$, pH 6.9). The 6.6 ml solution was then layered on top of 3 ml 1.8 M Sucrose cushion buffer in a pre-chilled centrifugation tube (#344059, Beckman Coulter Optima). The mixture was centrifuged at 30,000 x g for 45 min at 4°C. The supernatant was removed, and the pellet was resuspended in 90 μl of pre-chilled resuspension buffer (10 mM Tris-HCl, 0.25 M Sucrose, 25 mM KCl, 1.5 mM $MgCl_2$, and 1.5 mM $CaCl_2$, pH 6.9).

Sequencing and data analysis—Isolated nuclei were diluted in nuclease-free water to achieve a concentration of 700–1200 nuclei/ml and single nuclei were captured for cDNA library generation using a microfluidics platform (10x Genomics). Samples were prepared for sequencing using Chromium Single Cell 3’ Reagents Kits v3 (10x Genomics). The libraries were sequenced using NovaSeq 6000 (NovogeneAIT Genomics, Singapore). Sample demultiplexing, read alignment and counting of barcodes and unique molecular identifiers (UMIs) were performed using Cell Ranger (v_3.1.0; 10x Genomics). For quality control of the sequencing data, we used SoupX to correct raw counts for contamination by ambient RNA from the nuclei suspension (e.g. mitochondrial RNA)[46]. We then filtered

out barcodes with fewer than 1000 UMIs, fewer than 450 detected genes or more than 5% mitochondrial genes with Seurat (v3.2)[47].

Next, we performed UMI normalization, highly variable gene selection and scaling following the Seurat pipeline. For each of our 4 samples, 35 principal components (PCs) were used for uniform manifold approximation and projection (UMAP) and construction of a shared nearest neighbour (SNN) graph. Clustering was performed using the Louvain algorithm[48,49]. After removal of potential multiplets using DoubletFinder (v_2.0.3)[46,50], each sample was processed with SCTransform to control for sequencing depth and reduce technical noise[51]. Samples were integrated using the SCT workflow with 3000 features and 40 PCs. Processing steps were repeated as described above (40 PCs, res.=0.8)[52].Clusters were identified based on canonical markers expressed by specific cell types[53–56]. Clusters expressing markers of multiple cell types were removed [57,58]. Filtered data (34,144 genes, 21,494 cells) were then reprocessed and a UMAP plot was generated.

The vGluT2-expressing cluster (520 cells) was isolated for subclustering and further filtered to remove Gad2+ inhibitory neurons and vGluT2+ Mog+ oligodendrocyte subclusters, retaining 480 cells. SCTransform was then applied using 3000 variable genes. PCA, UMAP generation, SNN graph construction, and Louvain clustering were repeated as described above, using 50 PCs and a range of clustering resolutions from 0.3–1.3. A resolution of 0.5 was used to identify cluster marker genes and generate plots for publication. To understand the strongest contributors to variability within the DCN vGluT2 population, we examined the top principal components in greater detail. We extracted the loadings for each gene and embeddings values for each cell to identify the genes most strongly associated with the top PCs and their in-silico expression patterns.

Multiplexed fluorescent *in situ* hybridization

Refed and food deprived mice (n=3 mice per group) were anesthetized, transcardially perfused and brains were harvested, as described above, followed by 24-hour post-fixation in 4% PFA at 4°C. Brains were transferred and incubated in 30% sucrose for 40 hours at 4°C. Next, the brains were placed in plastic molds (Cat# 18986 Peel-A-Way disposable Embedding Molds T-12, Polysciences, Inc.), embedded in OCT (Cat 4585 Tissue Plus O.C.T. Compound Clear, Scigen Scientific Inc.) and frozen on dry ice. Coronal sections of 12 μm thickness were cut at −20°C on a cryostat (Leica, CM3050 S) and collected on glass slides (Fisherbrand Superfrost Plus Microscope Slides, Fisher Scientific, CAT 12–550-15). Fluorescent multiplex assays (ACDBio) were conducted based on manufacture's protocol (Wang et al., 2012). Briefly, tissue sections were fixed in 4% PFA, dehydrated in graded concentration of ethanol (50%, 70% and 100%), and treated in protease. Treated sections were hybridized to *Celf4*, *Crhr1*, *Dpp10*, *Esrrb*, *Miat*, *vGluT2*, *Homer1a*, *Spp1*, *Unc5d* and *vGAT* probes (RNAscope® ProbeMm-Celf4-C4 - Cat No. 512341-C4, RNAscope® Probe - Mm-Crhr1-C2 Cat No. 418011-C2, RNAscope® Probe – Mm-Dpp10 Cat No. 553331, RNAscope® Probe - Mm-Esrrb-C3 Cat No. 565951-C3, RNAscope® Probe Mm-Miat Cat No. 432521, RNAscope® Probe- Mm-Slc17a6 Cat No. 428871, RNAscope® Probe- Mm-Homer1-tvS-C2 Cat No. 433941-C2, RNAscope® Probe - Mm-Spp1 - Cat No. 435191, RNAscope® Probe - Mm-Spp1-C3 Cat No. 435191-C3, RNAscope® Probe -

Mm-Unc5d-C2 Cat No. 480461-C2, RNAscope® Probe- Mm-Slc32a1-C3 Cat No. 319191-C3), then incubated with corresponding amplification and detection solutions. HiPlex probe was used for *GlyT2* (RNAscope HiPlex Probe - Mm-Slc6a5-T8 – Cat No. 409741-T8) hybridization. Tissues were imaged and signals were cleaved prior to proceeding with multiplex fluorescent *in situ* hybridization for other probes. Finally, tissues were counterstained with Dapi, mounted (Fluoro-Gel, 17985–10) and cover slipped. Images of stained tissues were taken using upright microscope (Leica DM6 with Leica TCS SPE scan head, and Leica EL6000 for external light source) with 20x objective (0.80 NA). Images were taken in the linear range of the detector to avoid signal saturation (LASX v_3.7.4). Fluorescence signals in each cell were measured as raw integrated density using NIH ImageJ (version 1.50g, 1.52a; NIH). To determine the levels of expression in each cell, we used the following procedure. The *Mean background integrated density* was derived by averaging the mean integrated density measured from 5 different areas of the image that excluded strong positive cells. *Background in each cell* was calculated by multiplying *mean background integrated density value* to the area measured for each cell. The *integrated density of gene expression* was determined by subtracting the *background in each cell* from raw values of measured integrated density. To quantify *Homer1a*+ neurons, a threshold of 1000 integrated density value was statistically derived – Homer1a expression from food deprived and refed, glutamatergic and GABAergic neurons were grouped into bins of 500 integrated density value. A two-way ANOVA and post-hoc Holm-Sidak's multiple comparisons was applied (interaction $p<0.001$, main effect $p<0.001$, post hoc comparison to food deprived GABAergic neurons $p<0.001$, food deprived glutamatergic neurons $p=0.030$, refed GABAergic neurons $p<0.001$).

Gastric catheter implantation

Catheters were implanted as we have previously described[18,38,59]. Mice were anesthetized using 1.5–3% isoflurane with 1 L/minute oxygen flow. Subcutaneous injections of meloxicam (5 mg/Kg), bupivacaine (2 mg/Kg) and buprenorphine SR (1 mg/Kg) were provided. Surgeries were conducted in sterile conditions. An incision through the skin and muscle tissues was made along the abdominal midline. A hole was punctured through the fundus of the stomach to allow a Micro-Renathane catheter tubing (7 mm length, Braintree Scientific, MRE-033) with epoxy balls on both ends (Devcon Clear Epoxy Adhesive, 92926, Lowes) to be inserted and held in position with surgical mesh (5 mm diameter piece, Bard, 0112660). An intrascapular incision was made to allow the opposite end of the tubing to exit the body. To ensure the tubing remains sterile, a metal cap was inserted to reversibly close the tubing. Post-surgery, the tubing was flushed with sterile water to ensure passage and crushed chow pellets softened with water was provided *ad libitum* to the mice during a 1-week recovery period. Mice were singly caged post-surgery to avoid damage to gastric catheters. The weight of mice was measured daily, and experimentation began only after recovery of body weight to pre-surgical weight.

FosTRAP analysis

Effects of intragastric infusion on FosTRAP recombination: Gastric catheters were implanted into *TRAP2*; *Ai9* mice. Mice were fully habituated to experiment procedures for 3 consecutive days. Food deprived mice were intraperitoneally injected

with 50 mg/Kg of 4-hydroxytamoxifen (dissolved in ethanol and diluted in corn oil, and subsequent removal of ethanol by evaporation) 1.5 hours prior to IG infusion of 1 ml of distilled water or 1 ml of 1 kcal Ensure. The infusion rate was 1 ml/10 minutes and animals were returned to home cage 1.5 hours after the end of the infusion.

Effects of refeeding on FosTRAP recombination: Food deprived mice were injected with 50 mg/Kg of 4-hydroxytamoxifen via intraperitoneal injection 4 hours prior to ad libitum access to chow in home cage.

Statistics and reproducibility

Data were presented as means ± SEMs in figures and text. Two-tailed t-test were used for paired and unmatched comparisons. Multiple comparisons were conducted using one-way, two-way, or repeated measures ANOVAs. Test, statistics, significance levels, and sample sizes for each experiment are listed in Supp. Data Table 1. Statistical significance for t-tests and post-hoc comparisons are expressed as *$p<0.05$, **$p<0.01$, ***$p<0.001$; interaction: ∞$p<0.05$, ∞∞$p<0.01$, ∞∞∞$p<0.001$; main effect (group, condition, or treatment): ¤<0.05, ¤¤$p<0.01$, ¤¤¤$p<0.001$.

All statistical computations were performed using GraphPad Prism version 7.00 and 8.00 (GraphPad Software, USA).

Reproducibility of results from representative experiments: Fig. 1c, d, Extended data Fig. 6a–h; experiment repeated twice, n=3 mice/group each experiment. Extended Data Fig. 2d–I, k–bb; experiment conducted once on n=9 mice. Extended Data Fig. 3d; experiment repeated twice, n=3 or more mice each experiment. Extended Data Fig. 7e, f, g–l, Extended Data Fig. 8a–r; experiment conducted once on n=3 mice. Extended Data Fig. 8v, w; experiment conducted once on n=7 mice. Extended Data Fig. 9b, c; experiment conducted once on n=11 mice. Extended Data Fig. 10b; experiment repeated four times, n=6, 6, 7, 6 mice. Extended Data Fig. 11b–d, Extended Data Fig 12n–p; experiment conducted once on n=3 mice. Extended Data Fig. 12b–c; experiment conducted once on n=8 mice.

General Experimental Design: For each experiment, our subject numbers were determined by our pilot studies, laboratory publications, and power analyses (power=0.8, significance level=0.05, effect sizes=10–30%). For within-subject behavioural and fibre photometry analyses, all mice received all experimental conditions using a counterbalanced experimental design, where mice were randomly grouped for CNO and vehicle trials. For between-subject analyses, mice were randomly assigned to experimental condition. All behavioural and fibre photometry experiments, were performed by researchers blinded to experimental conditions. For histological experiments, protein intensities and neuron counts were quantified by histology assistants that were blinded to experimental condition. For all behavioural and fibre photometry experiments, virus expression, fibre placements, and/or cannula placements were verified post-mortem, and any mice with viral expression or implants outside of the area of interest were excluded from all analyses.

Materials availability

This study did not generate any new unique reagents. Mouse lines used in this study are on deposit at Jackson Labs and listed under Mice.

Extended Data

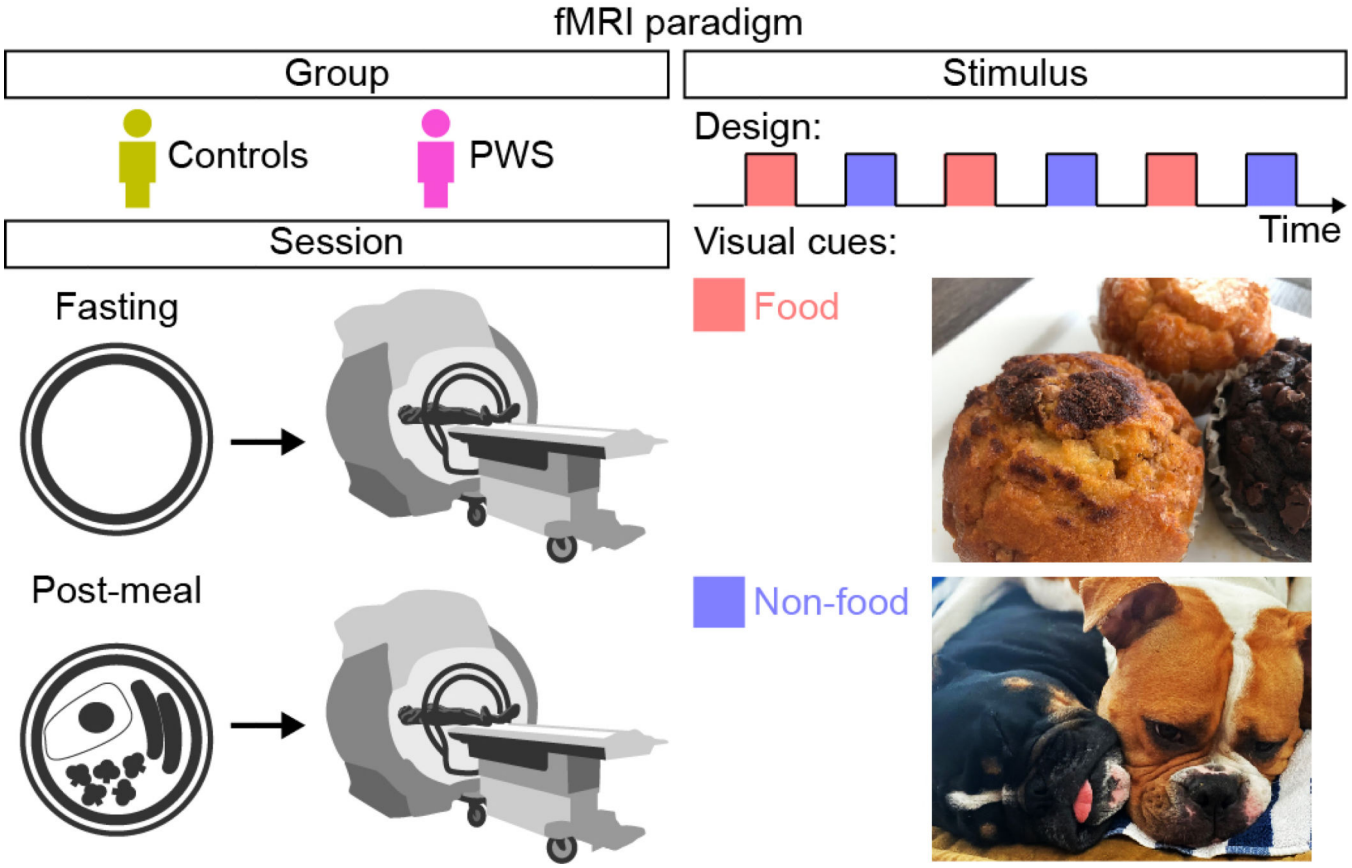

Extended Data Fig. 1 |. fMRI paradigm for response to food cue

Subjects with Prader-Willi syndrome (PWS) and controls underwent two separate scanning sessions (top left, group): either during fasting or post-meal (bottom left, session). During each scanning session, participants were presented with visual cues that alternate between food (muffin) and non-food (dog) categories (right, stimulus)[8].

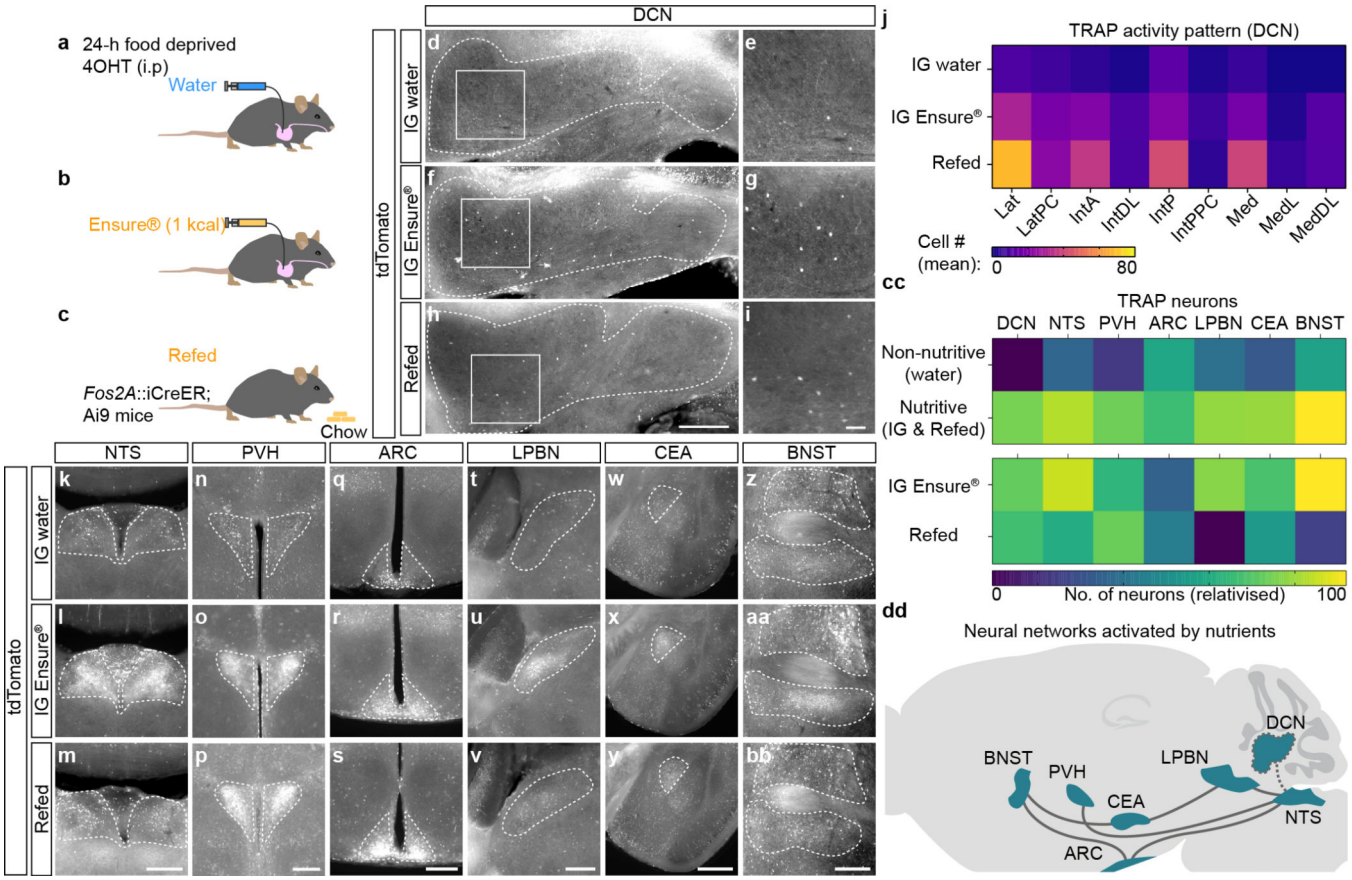

Extended Data Fig. 2 |. Neural activation pattern following food infusion and refeeding in mice

(a-c) Experimental design for Targeted Recombination of Activated Populations (TRAP) labelling of neurons activated by water infusion (IG water), Ensure® infusion (IG Ensure®) or refeeding (Refed) in *Fos2A*::iCreER; *Ai9* mice.

(d-i) tdTomato expression in the DCN after water infusion (d; e, magnified of box in d), 1 kcal Ensure® infusion (f; g, magnified of box in f), and chow refeeding (h; i, magnified of box in h). Scale bar, 500 μm (d, f, h), 100 μm (e, g, i).

(j) Heatmap depicting the activated cells recombined in DCN subregions following infusion and refeeding (n=9).

(k-m) tdTomato expression in the nucleus tractus solitarius (NTS) 3 weeks after water infusion (k), 1 kcal Ensure® infusion (l), and chow refeeding (m). Scale bar, 500 μm.

(n-p) tdTomato expression in the paraventricular hypothalamic nucleus (PVH) 3 weeks after water infusion (n), 1 kcal Ensure® infusion (o), and chow refeeding (p). Scale bar, 250 μm.

(q-s) tdTomato expression in the arcuate hypothalamic nuclei (ARC) 3 weeks after water infusion (q), 1 kcal Ensure® infusion (r), and chow refeeding (s). Scale bar, 250 μm.

(t-v) tdTomato expression in the lateral parabrachial nucleus (LPBN) 3 weeks after water infusion (t), 1 kcal Ensure® infusion (u), and chow refeeding (v). Scale bar, 250 μm.

(w-y) tdTomato expression in the central amygdaloid nucleus (CEA) 3 weeks after water infusion (w), 1 kcal Ensure® infusion (x), and chow refeeding (y). Scale bar, 500 μm.

(z-bb) tdTomato expression in the bed nucleus of the stria terminalis (BNST) 3 weeks after water infusion (z), 1 kcal Ensure® infusion (aa), and chow refeeding (bb). Scale bar, 250 μm.

(cc) Heatmap depicting relative density of cells recombined following water and calorie intake (top), and 1 kcal Ensure® infusion and refeeding (bottom, n=9).

(dd) Schematic depicting the DCN and key feeding brain regions that sense food cues and nutrients[60].

Statistical analysis in Supplementary Table 1.

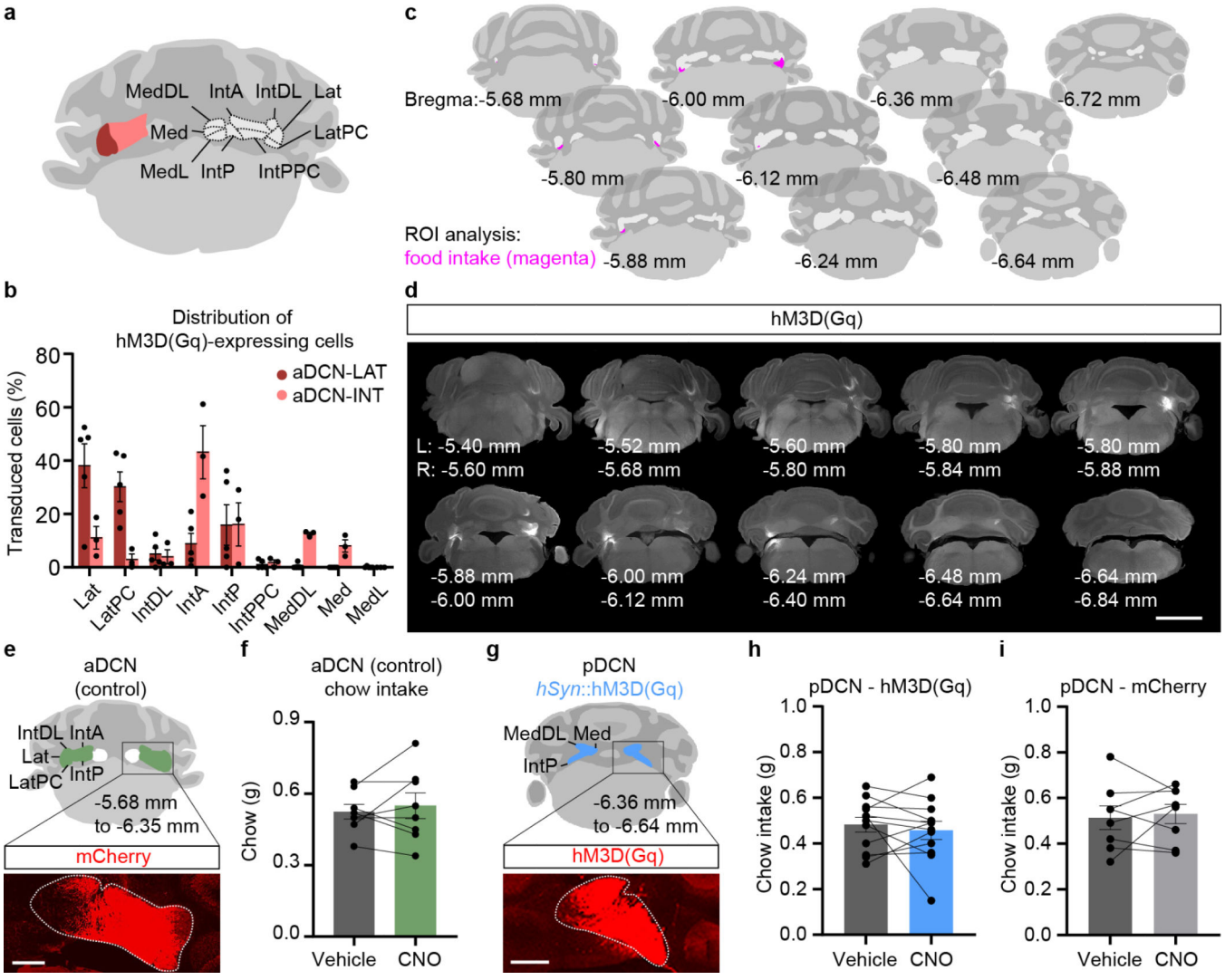

Extended Data Fig. 3 |. Mapping the DCN subregions that suppress food intake

(a) Schematic of the deep cerebellar nuclei. The lateral subnuclei of the anterior deep cerebellar nuclei (aDCN) are depicted in maroon (aDCN-LAT, consisting of Lat and LatPC, bregma −5.68 to −5.88 mm), interposed subnuclei of the aDCN are depicted in pink (aDCN-INT, consisting of IntA, IntDL, IntP, and IntPPC, bregma −6.00 to −6.35 mm). The posterior DCN is in grey (pDCN, consisting of IntP, IntPPC, Med, MedDL, and MedL, bregma −6.36 to −6.64 mm, see also e and g).

(b) Distribution of cells expressing hM3D(Gq) across 9 DCN subnuclei in mice with hM3D(Gq) targeted to the lateral nucleus (aDCN-LAT) and mice with hM3D(Gq) targeted to the interposed nucleus (aDCN-INT). Mice with targeting to the LAT show a reduction in food intake following DREADD activation (aDCN-LAT in maroon, n=5 mice, and aDCN-INT in pink, n=3 mice).
(c) Schematised serial coronal sections depicting regions where hM3D expression results in food intake reduction (magenta).
(d) Representative images of the entire DCN in a aDCN-LAT hM3D(Gq) mouse with hM3D(Gq) expression in the lateral nucleus. Scale bar, 2000 μm.
(e) Expression of mCherry (as control viral vector) in the aDCN (red: mCherry). Scale bar, 500 μm.
(f) Chow intake in mice with mCherry expression in the aDCN following vehicle or CNO treatment (n=8, paired t-test, P=0.539).
(g) hM3D(Gq) expression in the pDCN (red: hM3D(Gq)). Scale bar, 500 μm.
(h) Chow intake in mice with hM3D(Gq) expression in the pDCN following vehicle or CNO treatment (n=12, paired t-test, P=0.548).
(i) Chow intake in mice with mCherry expression in the pDCN following vehicle or CNO treatment (n=8, paired t-test, P=0.722).
Data are expressed as mean ± SEM. Lat, lateral; LatPC, lateral parvicellular; IntDL, interposed dorsolateral; IntA, interposed anterior nucleus; IntP, interposed posterior; IntPPC, interposed posterior parvicellular; MedDL, medial dorsolateral; Med, medial; MedL, medial lateral. Statistical analysis in Supplementary Table 1.

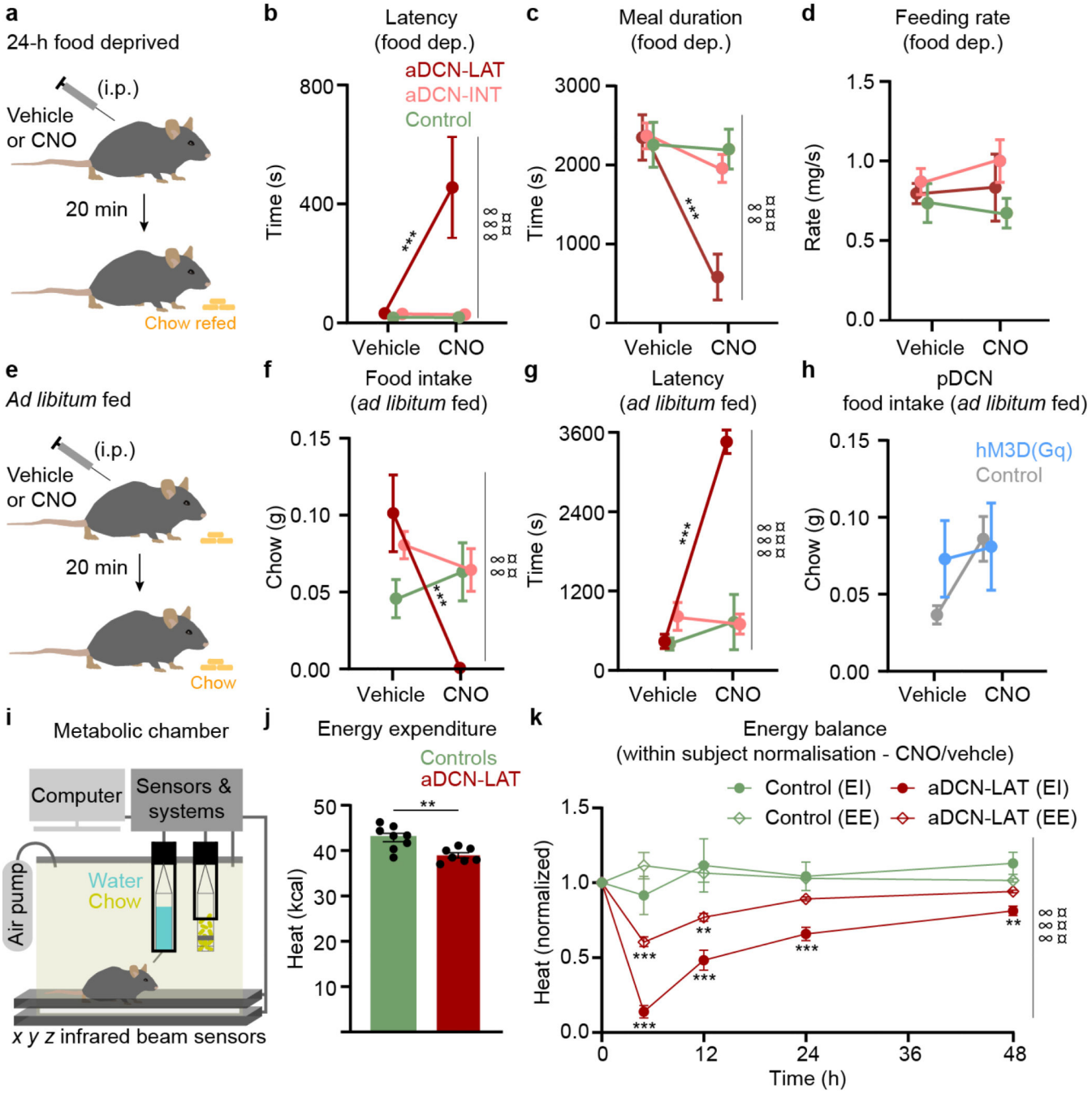

Extended Data Fig. 4 |. Neural activity in the aDCN suppresses food intake independent of hunger state with no compensatory metabolic changes

(a) Experimental design: meal pattern measurements of 24-h food-deprived mice following vehicle or CNO i.p. administration.

(b) Latency to first bite in food-deprived mice with hM3D(Gq) expression in the aDCN-LAT (n=9), aDCN-INT (n=16) or mCherry control in the aDCN (n=8) following vehicle or CNO treatment (two-way ANOVA interaction $P<0.001$, main effect $P=0.005$; Holm-Sidak's, $P<0.001$).

(c) Average meal duration during a 1-h chow intake assay following 24-h food deprivation in mice with hM3D(Gq) expression in the aDCN-LAT (n=9), aDCN-INT (n=16 mice), or control mCherry expression in the aDCN (n=8) following vehicle or CNO treatment (two-way ANOVA interaction P=0.005, main effect P<0.001; Holm-Sidak's, P<0.001).
(d) Rate of food intake during a 1-h chow intake assay following 24-h food deprivation in mice with hM3D expression in the aDCN-LAT (n=9), aDCN-INT (n=16), or control mCherry expression in the aDCN (n=8) following vehicle or CNO treatment (two-way ANOVA interaction P=0.748).
(e) Experimental design: meal pattern measurements of *ad libitum* fed mice following vehicle or CNO i.p. administration.
(f) Chow intake in *ad libitum* fed mice with hM3D(Gq) expression following vehicle or CNO treatment (aDCN-LAT: n=9, aDCN-INT: n=16, mCherry control: n=8; two-way ANOVA, interaction P=0.001, main effect P=0.006; Holm-Sidak's, P<0.001).
(g) Latency to first bite in *ad libitum* fed mice with hM3D(Gq) expression following vehicle or CNO treatment (aDCN-LAT: n=9, aDCN-INT: n=16, mCherry control: n=8; two-way ANOVA interaction P<0.001, main effect P<0.001; Holm-Sidak's, P<0.001).
(h) Chow intake in *ad libitum* fed mice with mCherry control or hM3D(Gq) expression in the pDCN following vehicle or CNO treatment (pDCN mCherry: n=8, pDCN hM3D(Gq): n=12; two-way ANOVA interaction P=0.358).
(i) Schematic of the metabolic monitoring experiment.
(j) Energy expenditure (kcal) over a 48-h period in mice with mCherry control (n=8) or hM3D(Gq) (n=7) expression in the aDCN-LAT (unpaired t-test, P=0.004).
(k) Energy intake (EI) and energy expenditure (EE) over 48-h period in mice with mCherry control or hM3D(Gq) expression in the aDCN-LAT following CNO treatment normalized to vehicle treatment (n=7 control, 8 aDCN-LAT-hM3D(Gq), repeated measures two-way ANOVA interaction P<0.001, main effect P<0.001; Holm-Sidak's, P<0.001, P=0.009 (EE); P<0.001, P<0.001, P<0.001, P=0.006 (EI)).
Data are expressed as mean ± SEM, two-sided P values, t-tests and post-hoc comparisons: **P<0.01, ***P<0.001, ANOVA interaction: ∞∞P<0.01, ∞∞∞∞P<0.001; ANOVA main effect of group: ¤¤P<0.01, ¤¤¤P<0.001. Statistical analysis in Supplementary Table 1.

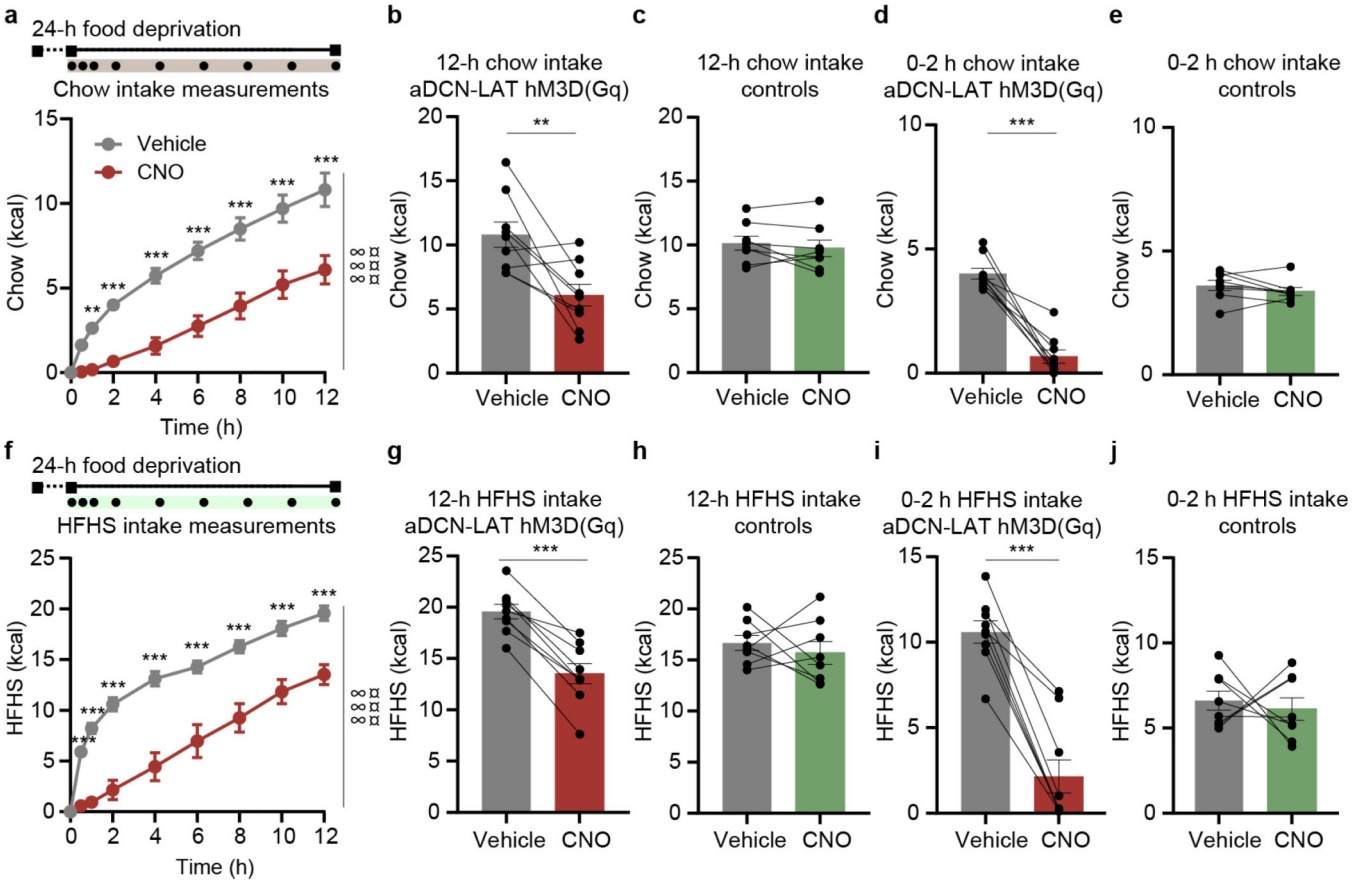

Extended Data Fig. 5 |. aDCN activity suppresses food intake regardless of hedonic value of food

(a) Experimental timeline: 24-h food deprivation followed by measurements of chow intake over 12-h (top). Cumulative kcal of chow intake in food-deprived mice with hM3D(Gq) expression in the aDCN-LAT following vehicle or CNO treatment (bottom; n=9 hM3D(Gq); repeated measures two-way ANOVA interaction $P<0.001$, main effect $P<0.001$; Holm-Sidak's, $P=0.094$ (30 min), $P=0.008$ (1 h), $P<0.001$ (2 h), $P<0.001$ (4h), $P<0.001$ (6h), $P<0.001$ (8 h), $P<0.001$ (10 h), $P<0.001$ (12 h)).

(b) 12-h food intake in food-deprived mice expressing hM3D(Gq) in the aDCN-LAT (n=9 mice, paired t-test, $P=0.008$).

(c) 12-h food intake in food-deprived mice expressing mCherry in the aDCN-LAT (n=8 mice, paired t-test, $P=0.391$).

(d) Food intake during the first 2-h of refeeding in food-deprived mice expressing hM3D(Gq) in the aDCN-LAT (n=9 mice, paired t-test, $P<0.001$).

(e) Food intake during the first 2-h of refeeding in food-deprived mice expressing mCherry in the aDCN-LAT (n=8 mice, paired t-test, $P=0.223$).

(f) Experimental timeline: 24-h food deprivation followed by measurement of high fat high sugar (HFHS) diet intake over 12 h (top). Cumulative kcal of HFHS diet intake in food-deprived mice with hM3D(Gq) expression in the aDCN-LAT following vehicle or CNO treatment (bottom; n= 9 hM3D(Gq) mice; two-way repeated measures ANOVA interaction $P<0.001$, main effect $P<0.001$; Holm-Sidak's, $P<0.001$ (30-min), $P<0.001$ (1-h), $P<0.001$ (2-h), $P<0.001$ (4-h), $P<0.001$ (6-h), $P<0.001$ (8-h), $P<0.001$ (10-h), $P<0.001$ (12-h)).

(g) 12-h HFHS diet intake in food-deprived mice expressing hM3D(Gq) in the aDCN-LAT (n=9 mice, paired t-test, $P<0.001$).
(h) 12-h HFHS diet intake in food-deprived mice expressing mCherry in the aDCN-LAT (n=8 mice, paired t-test, $P=0.527$).
(i) Calorie intake during the first 2-h of HFHS diet refeeding in food-deprived mice expressing hM3D(Gq) in the aDCN-LAT (n=9 mice, paired t-test, $P<0.001$).
(j) Calorie intake during the first 2-h of HFHS diet refeeding in food-deprived mice expressing mCherry in the aDCN-LAT (n=9 mice, paired t-test, $P=0.686$).
Data are expressed as mean ± SEM, two-sided P values, t-tests and post-hoc comparisons: $^{**}P<0.01$, $^{***}P<0.001$, ANOVA interaction: ∞∞∞∞$P<0.001$; ANOVA main effect of group: ¤¤¤$P<0.001$. Statistical analysis in Supplementary Table 1.

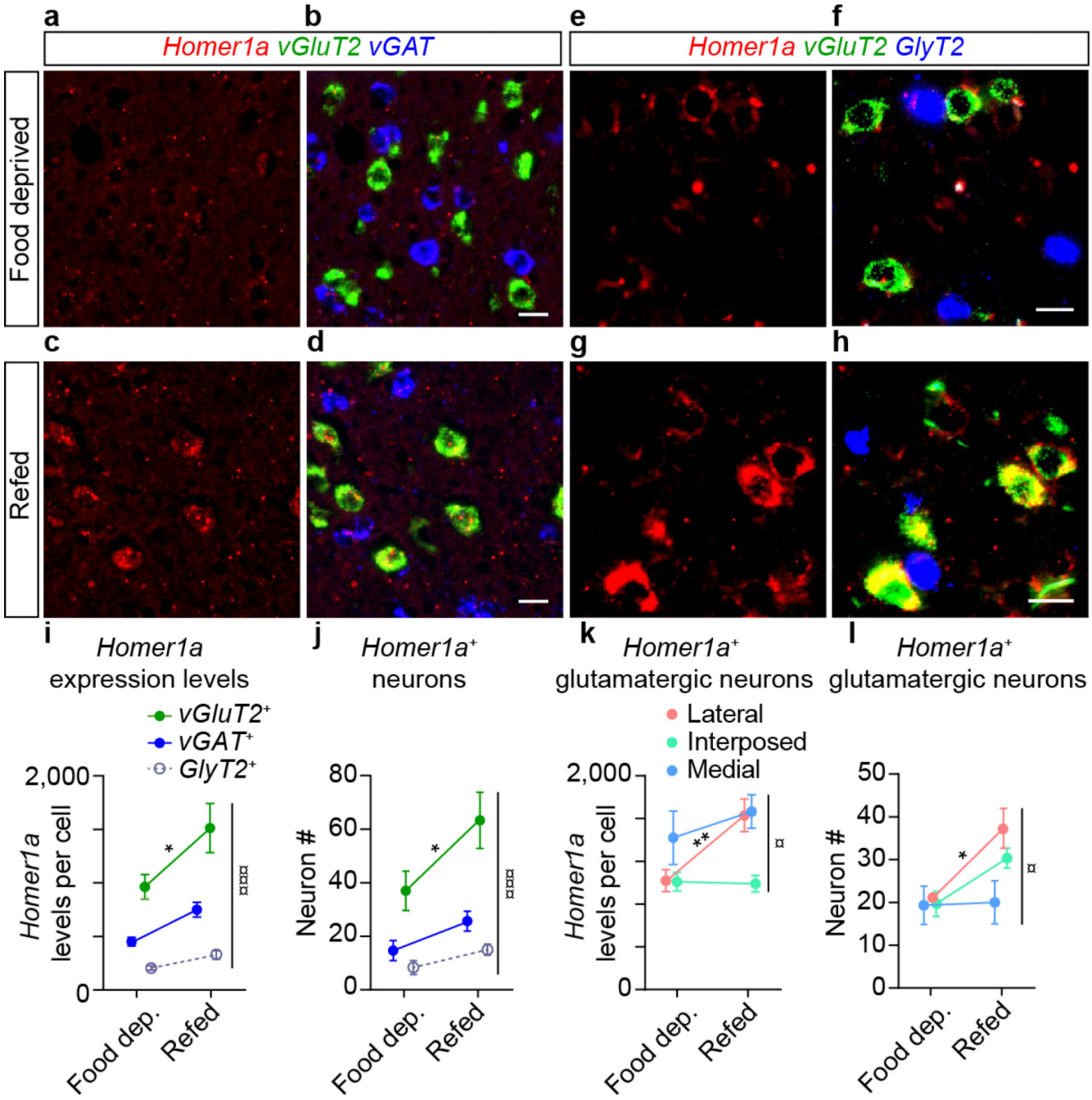

Extended Data Fig. 6 |. Glutamatergic neurons in the DCN are activated by food intake

(a-h) Fluorescent *In Situ* Hybridization (FISH) histochemistry in the lateral nucleus of the DCN in food-deprived (a, b, e, f) and chow-refed mice (c, d, g, h) (red, *Homer1a*; green, *vGluT2*; blue, *vGAT* in b and d, *GlyT2* in f and h). Scale bars, 20 μm.

(i) *Homer1a* expression in excitatory (*vGluT2*$^+$) and inhibitory (*vGAT*$^+$ or *GlyT2*$^+$) DCN neurons following food deprivation or refeeding (n=3 mice per group, two-way ANOVA main effect $P<0.001$; Holm-Sidak's, $P=0.034$).

(j) Number of excitatory (*vGluT2*$^+$) and inhibitory (*vGAT*$^+$ or *GlyT2*$^+$) DCN neurons that express *Homer1a* following food deprivation or refeeding (n=3 mice per group, two-way ANOVA main effect P=0.009; Holm-Sidak's, P=0.023).

(k, l) Expression level (k) and number (l) of *Homer1a*$^+$ *vGluT2*$^+$ neurons within the 3 major cerebellar nuclei following food deprivation or refeeding (n=3 mice per group, two-way ANOVA, expression level main effect P=0.013, number main effect P=0.010; Holm-Sidak's, expression level, P=0.006, number, P=0.025).

Data are expressed as mean ± SEM, two-sided P values, t-tests and post-hoc comparisons: *P<0.05, **P<0.01, ANOVA interaction: ∞∞∞∞P<0.001; ANOVA main effect of group: ¤P<0.05, ¤¤¤P<0.001. Statistical analysis in Supplementary Table 1.

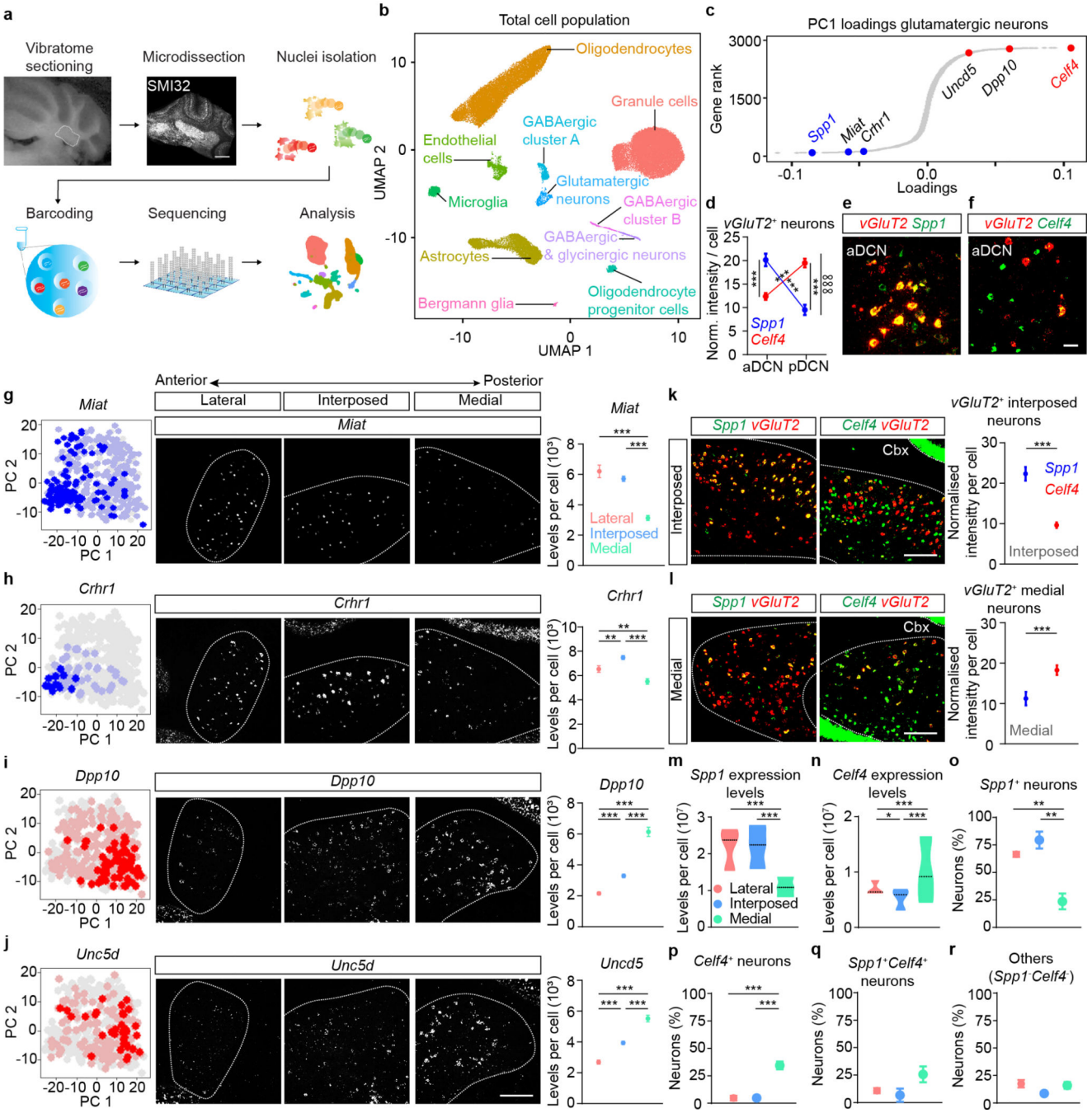

Extended Data Fig. 7 |. Gene expression gradient along the anterior-posterior axis of the DCN

(a) Experimental design of single nucleus RNA sequencing of DCN neurons.

(b) Uniform Manifold Approximation and Projection for Dimension Reduction (UMAP) plot of cerebellar cell types derived from microdissection of the DCN and surrounding tissues.

(c) Principal component (PC) 1 loadings of select class I and class II defining genes expressed by *vGluT2*+ DCN neurons.

(d) *Celf4* (red) and *Spp1* (blue) expression level in *vGluT2+* neurons in the DCN, 492 neurons (two-way ANOVA interaction $P<0.001$; Holm-Sidak's, $P<0.001$, $P<0.001$, $P<0.001$, $P<0.001$).
(e, f) *vGluT2* (red, e, f), *Spp1* (green, e) and *Celf4* (green, f) expression in the aDCN. Scale bar, 25 μm.
(g) PC embedding of *Miat* expression, fluorescent in situ hybridization (FISH) and quantification of *Miat* levels in *vGluT2*$^+$ neurons in the three major cerebellar nuclei (n=1,434 neurons, one-way ANOVA $P<0.001$; Holm-Sidak's, $P=0.165$, $P<0.001$, $P<0.001$).
(h) PC embedding of *Crhr1* expression, FISH, and quantification of *Crhr1* levels in *Miat*$^+$ neurons in the three major cerebellar nuclei (n=1,434 neurons, one-way ANOVA $P<0.001$; Holm-Sidak's, $P=0.003$, $P=0.006$, $P<0.001$).
(i) PC embedding of *Dpp10* expression, FISH, and quantification of *Dpp10* levels in *Celf4*$^+$ neurons in the three major cerebellar nuclei (n=2,261 neurons, one-way ANOVA $P<0.001$; Holm-Sidak's, $P<0.001$, $P<0.001$, $P<0.001$).
(j) PC embedding of *Unc5d* expression, FISH, and quantification of *Unc5d* levels in *Celf4*$^+$ neurons in the three major cerebellar nuclei (n=2,261 neurons, one-way ANOVA $P<0.001$; Holm-Sidak's, $P<0.001$, $P<0.001$, $P<0.001$). Scale bar, 100 μm.
(k) FISH of *Spp1 and Celf4* expression in *vGluT2*$^+$ neurons of the interposed nucleus (left image: red, *vGluT2*; green, *Spp1*; right image: red, *vGluT2*; green, *Celf4*; n=3, unpaired t-test, $P<0.001$). Scale bar,100 μm.
(l) FISH of Spp1 and *Celf4* expression in *vGluT2*$^+$ neurons in the medial nucleus (left image: red, *vGluT2*; green, *Spp1*; right image: red, *vGluT2*; green, *Celf4*; n=3, unpaired t-test, $P<0.001$). Scale bar, 100 μm.
(m) *Spp1* expression levels in *vGluT2*$^+$ neurons across the three major cerebellar nuclei (n=3, one-way ANOVA $P<0.001$; Holm-Sidak's, $P=0.946$, $P<0.001$, $P<0.001$).
(n) *Celf4* expression levels in *vGluT2*$^+$ neurons across the three major cerebellar nuclei (n=3, one-way ANOVA $P<0.001$; Holm-Sidak's, $P=0.026$, $P<0.001$, $P<0.001$).
(o-r) Quantification of *Spp1*$^+$ (o), *Celf4*$^+$ (p), *Spp1*$^+$*Celf4*$^+$ (q) and *Spp1*$^-$*Celf4*$^-$ (r) *vGluT2*$^+$ neurons across the three major cerebellar nuclei (n=3, one-way ANOVA (o) $P=0.002$, (p) $P<0.001$; Holm-Sidak's, (o) $P=0.190$, $P=0.005$, $P=0.002$, (p) $P=0.982$, $P<0.001$, $P<0.001$, lateral versus interposed, lateral versus medial, and interposed versus medial, respectively). Data are expressed as mean ± SEM, two-sided *P* values, post-hoc comparisons: *$P<0.05$, **$P<0.01$, ***$P<0.001$; ANOVA interaction: ∞∞∞∞$P<0.001$. Statistical analysis in Supplementary Table 1.

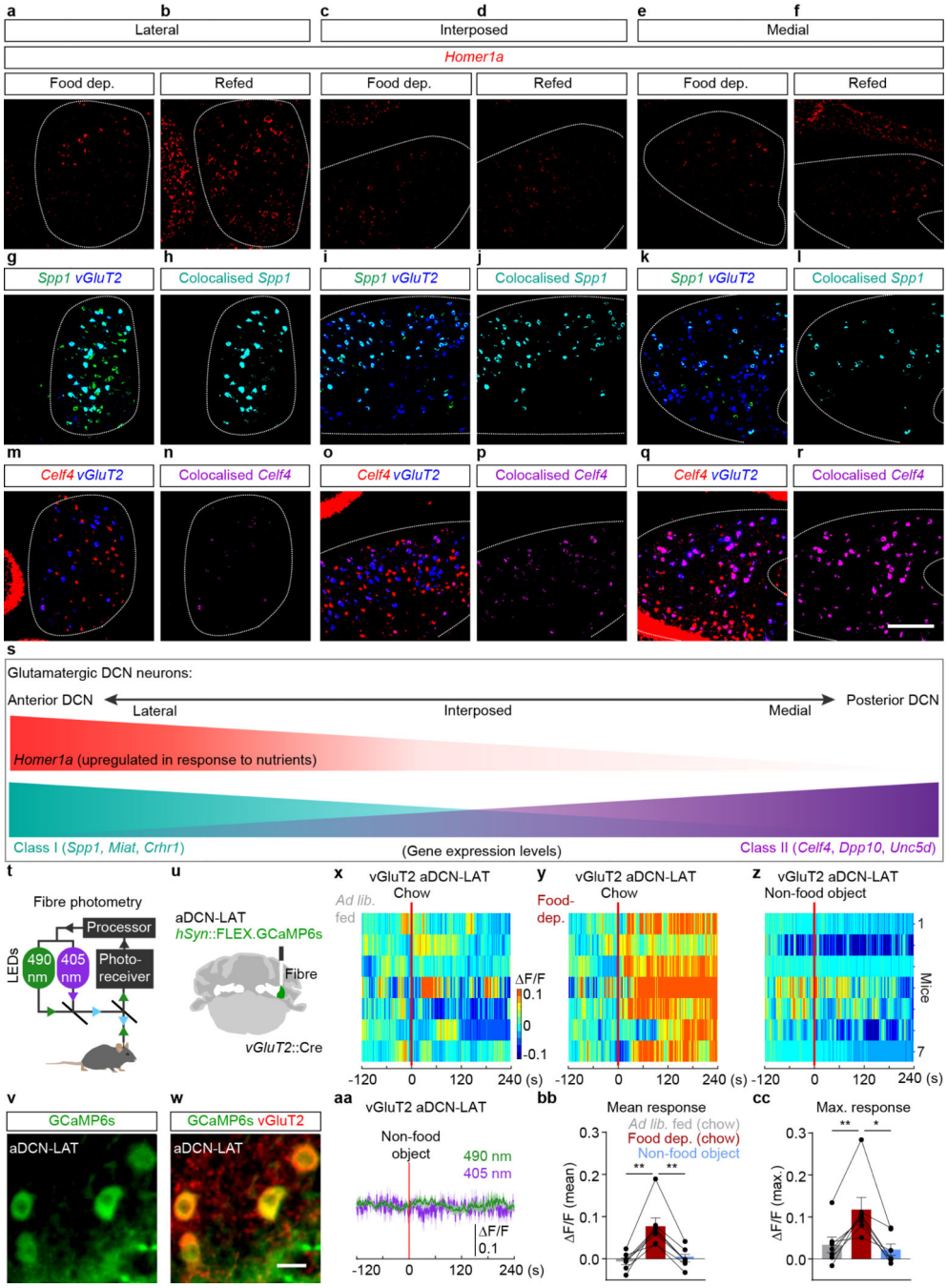

Extended Data Fig. 8 |. Molecular and topographical distinctions of DCN neurons that respond to food intake

(a-f) Expression of activity-regulated transcript *Homer1a*61 (red) in the three major cerebellar nuclei following food deprivation (a, c, e) or refeeding (b, d, f).

(g-l) *Spp1* expression (green) in *vGluT2*$^{+}$ neurons (blue) (g, i, k), and colocalised *Spp1* (cyan, *Spp1*$^{+}$ *vGluT2*$^{+}$ neurons) (h, j, l) in the three major cerebellar nuclei.

(m-r) *Celf4* expression (blue) in *vGluT2*$^{+}$ neurons (red) (m, o, q), and colocalised *Celf4* (magenta, *Celf4*$^{+}$ *vGluT2*$^{+}$ neurons) (n, p, r) in the three major cerebellar nuclei. Scale bar, 100 μm.

(s) Summary of the expression of *Spp1* and *Celf4* and the distribution of *Homer1a+* DCN neurons.
(t) Schematic of fibre photometry system.
(u-w) Fibre targeting aDCN-LAT glutamatergic neurons in *vGluT2*::Cre mouse (u), expression of GCaMP6s (green) and vGluT2 (red) (v, w). Scale bar, 20 μm.
(x-z) Heatmaps depicting ΔF/F of GCaMP6 signals in the aDCN-LAT glutamatergic neurons of *ad libitum* fed (x) and food-deprived (y) mice response to chow, and *ad libitum* fed mice response to non-food object (z, marble). Signals are aligned to the introduction of chow or non-food object (red line) (n=7 mice).
(aa) Average ΔF/F of GCaMP6 signals in the aDCN-LAT glutamatergic neurons (490 nm, green, and control 405 nm, magenta). Signals are aligned to the introduction of non-food object (red line). Dark line represents the mean and lighter shaded area represents SEMs (n=7).
(bb-cc) Mean (bb) and max (cc) ΔF/F GCaMP6s signals of aDCN-LAT glutamatergic neurons in response to chow, in *ad libitum* fed (grey) and food-deprived (red) mice, and response to non-food object in *ad libitum* fed mice (n=7, one-way ANOVA (bb) $P<0.001$, (cc) $P<0.001$; Holm-Sidak's, (bb) $P<0.006$, $P=0.475$, $P<0.003$, (cc) $P<0.009$, $P=0.651$, $P=0.011$, *ad libitum* fed chow versus food deprivation chow, *ad libitum* fed chow versus non-food, food deprivation chow versus non-food, respectively).
Data are expressed as mean ± SEM, two-sided *P* values, post-hoc comparisons: *$P<0.05$, **$P<0.01$. Statistical analysis in Supplementary Table 1.

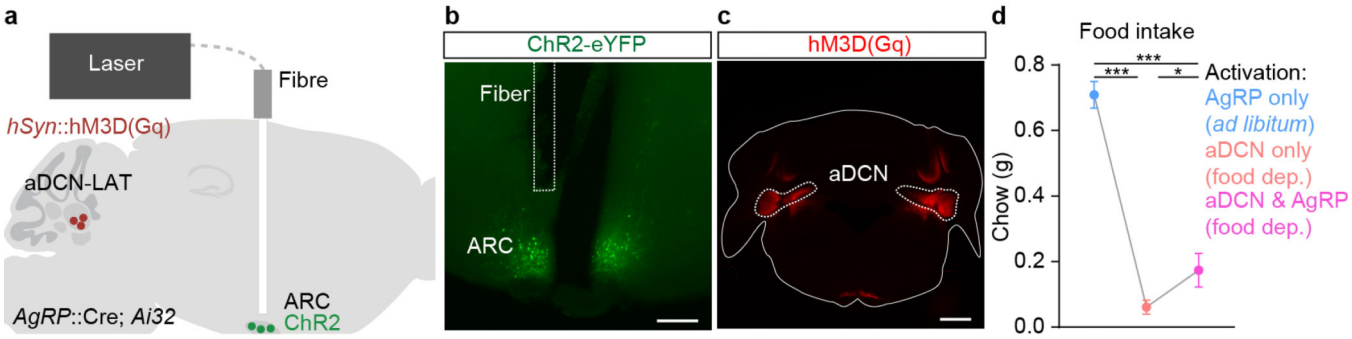

Extended Data Fig. 9 |. Activation of arcuate AgRP neurons does not fully restore food intake suppression mediated by aDCN-LAT activation

(a) Schematic depicting hM3D(Gq) expression in the aDCN-LAT, ChR2 expression and fibre implant in the arcuate nucleus (ARC) of a *AgRP*::Cre; *Ai32* mouse for either individual or simultaneous activation.
(b, c) ChR2-eYFP expression in AgRP ARC neurons (b) and hM3d(Gq) expression in the aDCN (c). Scale bar, 500 μm in b, 1000 μm in c.
(d) Chow intake following AgRP neuron activation in *ad libitum* state (blue), aDCN neuron activation in food-deprived state (red), or AgRP and aDCN neuron activation in food-deprived state (pink) (n=11, repeated measures one-way ANOVA, $P=0.001$; Holm-Sidak's, $P<0.001$, $P<0.001$, $P=0.024$).
Data are expressed as mean ± SEM, two-sided *P* values, post-hoc comparisons: *$P<0.05$, **$P<0.01$, ***$P<0.001$. Statistical analysis in Supplementary Table 1.

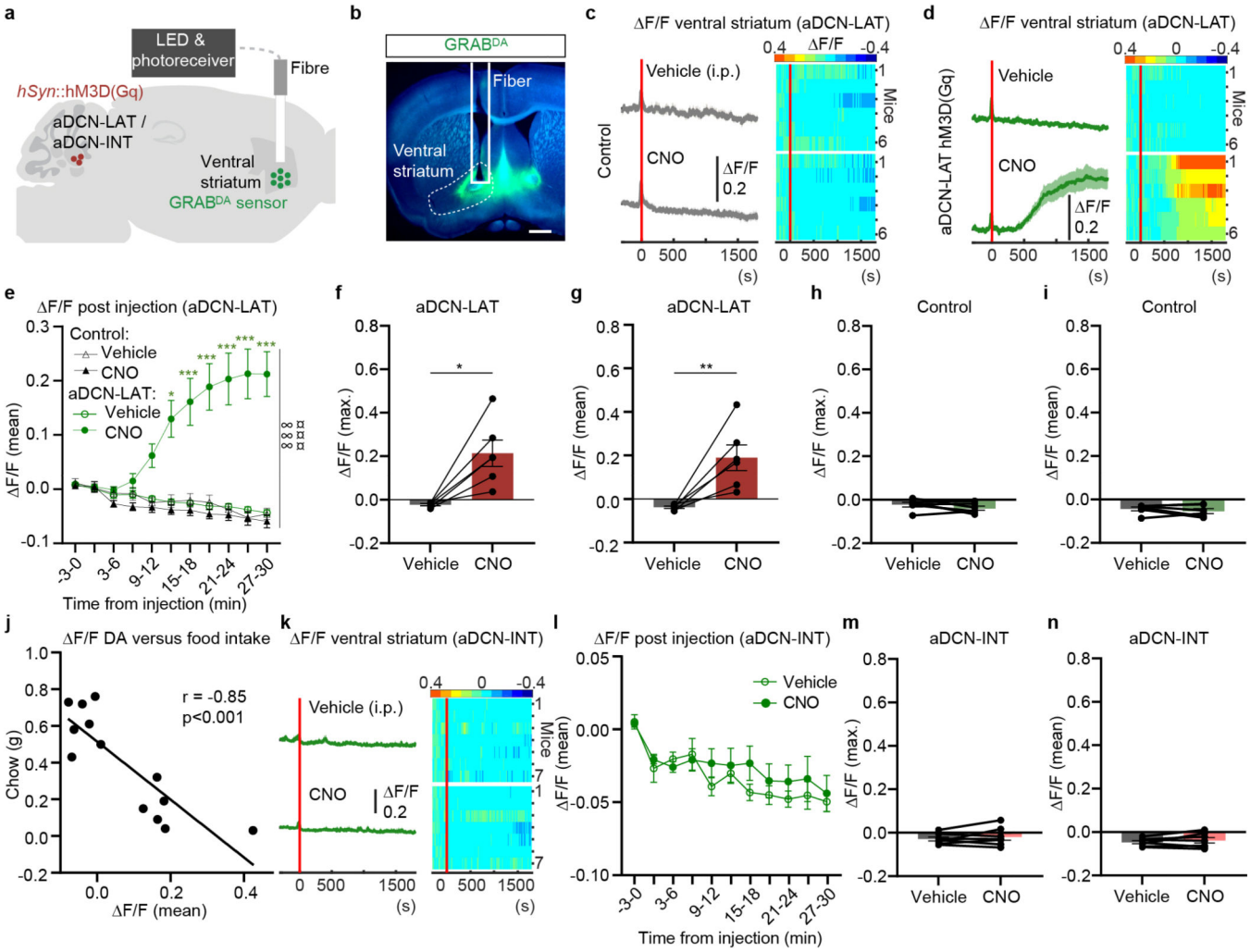

Extended Data Fig. 10 |. Activation of aDCN neurons robustly increases striatal dopamine signalling that correlates with reduced food intake

(a) Schematic depicting hM3D(Gq) expression in the DCN combined with GRAB^{DA} expression[40] and fibre implant in the ventral striatum which receives projections from the ventral tegmental area (VTA) dopamine (DA) neurons[62,63].

(b) GRAB^{DA} expression and fibre placement in the ventral striatum. Scale bar, 1000 μm.

(c, d) Average ΔF/F of GRAB^{DA} signals in the ventral striatum of food-deprived mCherry control (c) or aDCN-LAT hM3D(Gq) (d) mice treated with vehicle or CNO. Signals are aligned to the vehicle or CNO injection (red line). Dark line represents the mean and lighter shaded area represents SEMs. Corresponding heatmaps (right) depict ΔF/F of GRAB^{DA} signals in each mouse (n=6 control mice, grey; n=6 hM3D(Gq) aDCN-LAT mice, green).

(e) Average ΔF/F of GRAB^{DA} signals in 3-min bins (n=6 control mice, grey; n=6 hM3D(Gq) aDCN-LAT mice, repeated measures two-way ANOVA interaction P<0.001, main effect P<0.001; Holm-Sidak's, P=0.027/=0.397/=0.625 (12–15 min), P<0.001/<0.001/<0.001 (15–18 min), P<0.001/<0.001/<0.001 (18–21 min), P<0.001/<0.001/<0.001 (21–24 min), P<0.001/<0.001/<0.001 (24–27 min), P<0.001/<0.001/<0.001 (27–30 min), hM3D(Gq) CNO to hM3D(Gq) vehicle/control CNO/control vehicle respectively).

(f) Maximum ΔF/F of $GRAB^{DA}$ signals in the ventral striatum of vehicle or CNO treated food-deprived mice with aDCN-LAT hM3D(Gq) (n=6, paired t-test, P=0.011).
(g) Mean ΔF/F of $GRAB^{DA}$ signals in the ventral striatum (n=6, paired t-test, P=0.002).
(h) Maximum ΔF/F of $GRAB^{DA}$ signals in the ventral striatum of vehicle or CNO treated food-deprived mice with aDCN mCherry control mice (n=6, paired t-test, P=0.242).
(i) Mean ΔF/F of $GRAB^{DA}$ signals in the ventral striatum of vehicle or CNO treated food-deprived mice with aDCN mCherry control mice (n=6, paired t-test, P=0.418).
(j) Scatter plot comparing changes in $GRAB^{DA}$ signals to amount of chow consumed in 1 h following activation of the aDCN in hM3D(Gq)-expressing mice treated with CNO (n=13, Pearson correlation).
(k) Average ΔF/F of $GRAB^{DA}$ signals in the ventral striatum of food-deprived aDCN-INT hM3D(Gq) mice treated with vehicle or CNO. Signals are aligned to the vehicle or CNO injection (red line). Dark line represents the mean and lighter shaded area represents SEMs. Corresponding heatmaps (right) depict ΔF/F of $GRAB^{DA}$ signals in each mouse (n=7).
(l) Average ΔF/F of $GRAB^{DA}$ signals in 3-min bins following vehicle or CNO treatment of the aDCN-INT with hM3D(Gq) (n=7, repeated measures two-way ANOVA interaction P=0.301).
(m) Maximum ΔF/F of $GRAB^{DA}$ signals in the ventral striatum of vehicle or CNO treated food-deprived mice with aDCN-INT hM3D(Gq) mice (n=7, paired t-test, P=0.410).
(n) Mean ΔF/F of $GRAB^{DA}$ signals in the ventral striatum of vehicle or CNO treated food-deprived mice with aDCN-INT hM3D(Gq) mice (n=7, paired t-test, P=0.367).
Data are expressed as mean ± SEM, two-sided P values, t-tests and post-hoc comparisons: *P<0.05, **P<0.01, ***P<0.001; ANOVA interaction: ∞∞∞∞P<0.001; ANOVA main effect of group: ¤¤¤P<0.001. Statistical analysis in Supplementary Table 1.

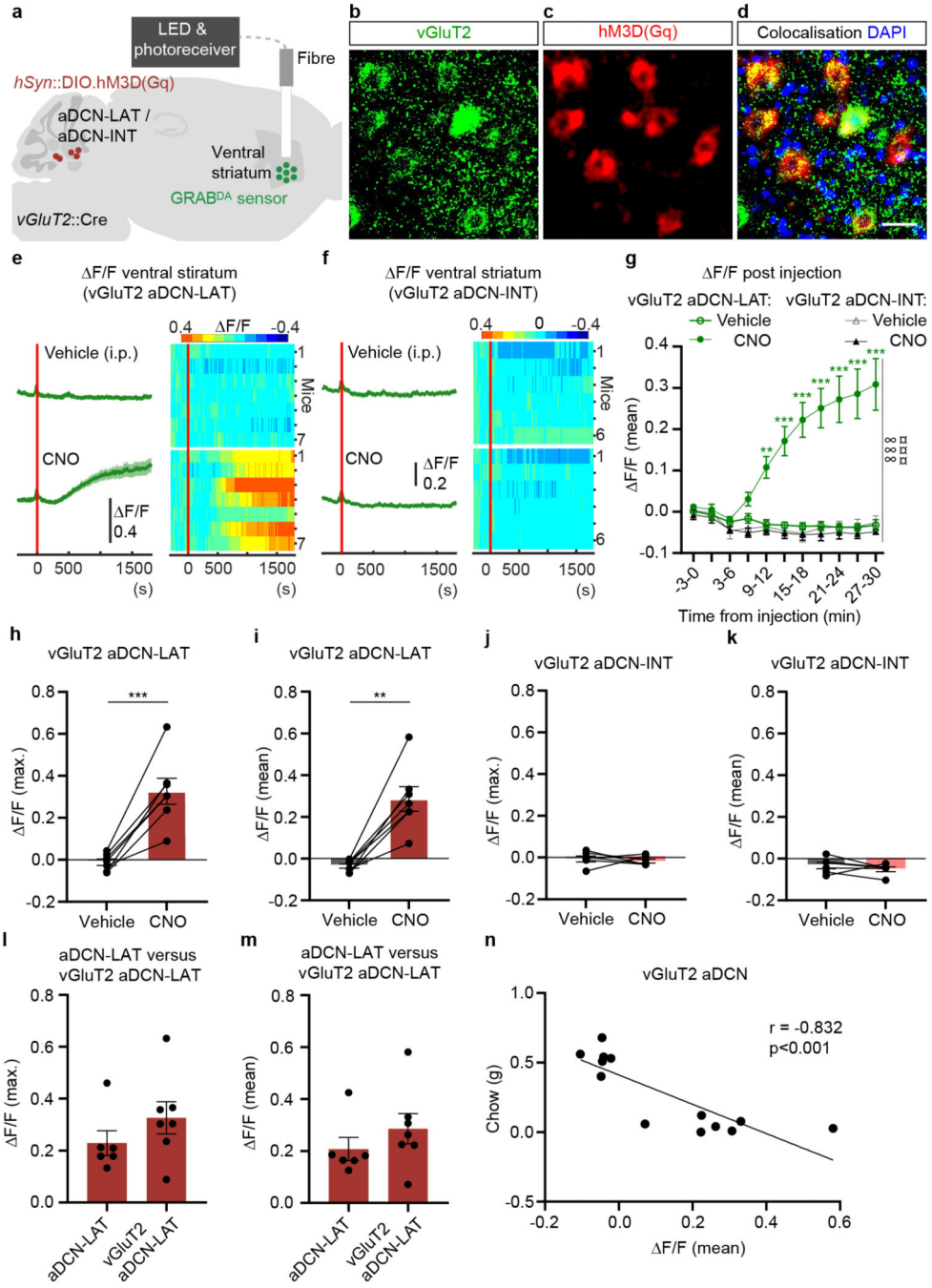

Extended Data Fig. 11 |. Selective activation of glutamatergic aDCN neurons is sufficient to induce striatal dopamine surge and suppression of food intake

(a) Schematic depicting hM3D(Gq) expression in the DCN combined with GRAB^{DA} expression and fibre implant in the striatum of a *vGluT2*::Cre mouse.

(b-d) IHC analysis of Cre dependent hM3D(Gq) expression in the DCN of *vGluT2*::Cre mouse (green, vGluT2, red, hM3D(Gq), blue, DAPI). Scale bar, 25 μm in b-d.

(e) Average ΔF/F of GRAB^{DA} signals in the ventral striatum of food-deprived mice expressing hM3D(Gq) in glutamatergic neurons of the aDCN-LAT following vehicle or CNO injection. Signals are aligned to the vehicle or CNO injection (red line). Dark line

represents the mean and lighter shaded area represents SEMs. Corresponding heatmaps (right) depict ΔF/F of $GRAB^{DA}$ signals in each mouse (n=7).

(f) Average ΔF/F of $GRAB^{DA}$ signals in the ventral striatum of food-deprived mice expressing hM3D(Gq) in glutamatergic neurons of the aDCN-INT following vehicle or CNO injection. Signals are aligned to the vehicle or CNO injection (red line). Dark line represents the mean and lighter shaded area represents SEMs. Corresponding heatmaps (right) depict ΔF/F of $GRAB^{DA}$ signals in each mouse (n=6).

(g) Average ΔF/F of $GRAB^{DA}$ signals in 3-min bins of food-deprived mice expressing hM3D(Gq) in glutamatergic neurons of the aDCN-INT or aDCN-LAT (n=7 vGluT2 aDCN-LAT mice, green, n=6 vGluT2 aDCN-INT mice, grey, two-way ANOVA, interaction $P<0.001$, main effect $P<0.001$; Holm-Sidak's, $P=0.001/=0.001/<0.001$ (9–12 min), $P<0.001/<0.001/<0.001$ (12–15 min), $P<0.001/<0.001/<0.001$ (15–18 min), $P<0.001/<0.001/<0.001$ (18–21 min), $P<0.001/<0.001/<0.001$ (21–24 min), $P<0.001/<0.001/<0.001$ (24–27 min), $P<0.001/ <0.001/<0.001$ (27–30 min), aDCN-LAT CNO to vehicle/aDCN-INT CNO/aDCN-INT vehicle respectively).

(h) Maximum ΔF/F $GRAB^{DA}$ signals in the ventral striatum of food-deprived mice expressing hM3D(Gq) in glutamatergic neurons of the aDCN-LAT following vehicle or CNO treatment (n=7, paired t-test, $P<0.001$).

(i) Mean ΔF/F $GRAB^{DA}$ signals in the ventral striatum of food-deprived mice expressing hM3D(Gq) in glutamatergic neurons of the aDCN-LAT following vehicle or CNO treatment (n=7, paired t-test, $P=0.001$).

(j) Maximum ΔF/F $GRAB^{DA}$ signals in the ventral striatum of food-deprived mice expressing hM3D(Gq) in glutamatergic neurons of the aDCN-INT following vehicle or CNO treatment (n=6, paired t-test, $P=0.644$).

(k) Mean ΔF/F $GRAB^{DA}$ signals in the ventral striatum of food-deprived mice expressing hM3D(Gq) in glutamatergic neurons of the aDCN-INT following vehicle or CNO treatment (n=6, paired t-test, $P=0.367$).

(l) Maximum ΔF/F $GRAB^{DA}$ signals in the striatum following non-specific aDCN-LAT activation or $vGluT2^{+}$ aDCN-LAT neuron activation (aDCN-LAT: n=6 mice, vGluT2 aDCN-LAT: n=7, unpaired t-test, $P=0.250$).

(m) Mean ΔF/F $GRAB^{DA}$ signals in the striatum of following non-specific aDCN-LAT activation or $vGluT2^{+}$ aDCN-LAT neuron activation (aDCN-LAT: n=6 mice, vGluT2 aDCN-LAT: n=7, unpaired t-test, $P=0.323$).

(n) Plot of $GRAB^{DA}$ signals and corresponding food intake in food-deprived mice treated following glutamatergic aDCN activation (n=13, Pearson correlation). Solid line indicates the linear trend line fit to the data.

Data are expressed as mean ± SEM, two-sided P values, t-tests and post-hoc comparisons: $^{**}P<0.01$, $^{***}P<0.001$; ANOVA interaction: ∞∞∞∞ $P<0.001$; ANOVA main effect of group: ¤¤¤ $P<0.001$. Statistical analysis in Supplementary Table 1.

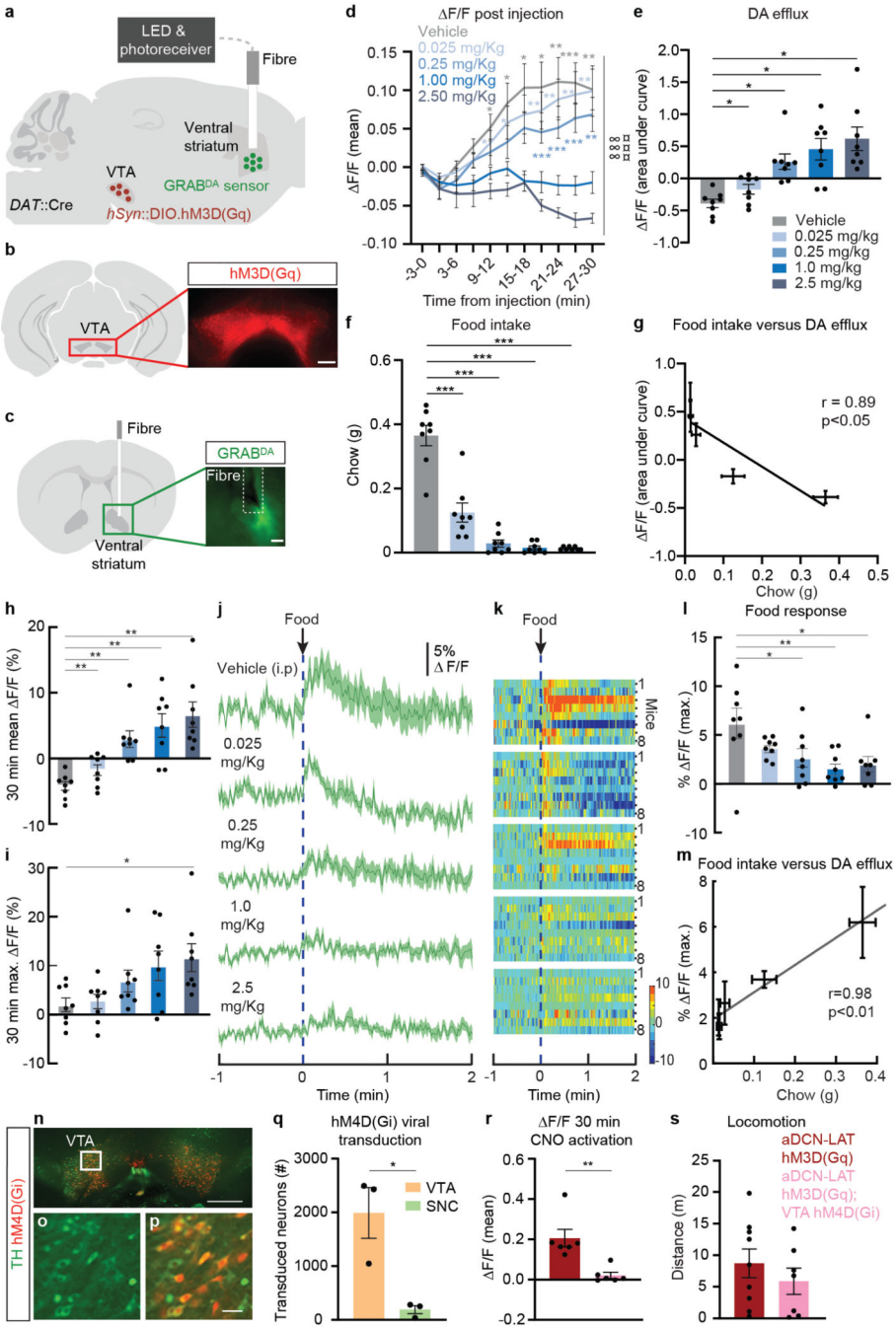

Extended Data Fig. 12 |. Increased striatal dopamine suppresses food intake

(a) Schematic depicting hM3D(Gq) expression in the VTA of a *DAT*::Cre mouse, and GRAB^{DA} expression and fibre implant in the ventral striatum.

(b-c) Representative images of hM3D(Gq) expression in the VTA (b), and GRAB^{DA} expression and fibre track in the ventral striatum (c) of a *DAT*::Cre mouse. Scale bar, 500 μm in B, 200 μm in C.

(d) Average ΔF/F of GRAB^{DA} signals in 3-min bins following VTA neuron activation with vehicle and varying concentrations of CNO (0.025 mg/Kg, 0.25 mg/Kg, 1 mg/Kg and 2.5

mg/Kg; n=8 per group, repeated measures two-way ANOVA interaction $P<0.001$, main effect $P<0.001$; Holm-Sidak's).

(e) Net area under curve ΔF/F of $GRAB^{DA}$ signals following VTA neuron activation with vehicle and varying concentrations of CNO (0.025 mg/Kg, 0.25 mg/Kg, 1 mg/Kg and 2.5 mg/Kg; n=8 per group, repeated measures one-way ANOVA $P<0.001$; Holm-Sidak's, $P=0.012$ (vehicle versus 0.025 mg/Kg), $P=0.010$ (vehicle versus 0.25 mg/Kg), $P=0.023$ (vehicle versus 1.0 mg/Kg), $P=0.010$ (vehicle versus 2.5 mg/Kg)).

(f) Food intake of food-deprived mice following VTA neuron activation with vehicle and varying concentrations of CNO (0.025 mg/Kg, 0.25 mg/Kg, 1 mg/Kg and 2.5 mg/Kg; n=8 per group, repeated measures one-way ANOVA $P<0.001$; Holm-Sidak's, $P<0.001$ (vehicle versus 0.025 mg/Kg), $P<0.001$ (vehicle versus 0.25 mg/Kg), $P<0.001$ (vehicle versus 1.0 mg/Kg), $P<0.001$ (vehicle versus 2.5 mg/Kg)).

(g) Plot of $GRAB^{DA}$ signals and corresponding food intake in food-deprived mice treated following VTA neuron activation (n=8 per group, Pearson correlation). Solid line indicates the linear trend line fit to the data.

(h) Average ΔF/F of $GRAB^{DA}$ signals from 0 to 30 min following treatment with vehicle and varying concentrations of CNO (n=8 per group, repeated measures one-way ANOVA $P<0.001$; Holm-Sidak's, $P=0.004$ (vehicle versus 0.025 mg/Kg), $P=0.004$ (vehicle versus 0.25 mg/Kg), $P=0.004$ (vehicle versus 1.0 mg/Kg), $P=0.004$ (vehicle versus 2.5 mg/Kg)).

(i) Maximum ΔF/F of $GRAB^{DA}$ signals following treatment with vehicle and varying concentrations of CNO (n=8 per group, repeated measures one-way ANOVA $P=0.023$; Holm-Sidak's, $P=0.034$ (vehicle versus 2.5 mg/Kg)).

(j) Average ΔF/F of $GRAB^{DA}$ signals during presentation of food in fasted mice following treatment with vehicle and varying concentrations of CNO (0.025, 0.25, 1.0 and 2.5 mg/Kg). Signals are aligned to food presentation. Dark lines represent mean values and lighter shaded areas represent SEM (n=8).

(k) Heatmaps reporting ΔF/F of $GRAB^{DA}$ signals in individual mice in (j) (n=8).

(l) Maximum ΔF/F of $GRAB^{DA}$ signals during food presentation in mice following treatment with vehicle and varying concentrations of CNO (n=8 per group, one-way ANOVA $P=0.0117$; Holm-Sidak's, $P=0.0389$ (vehicle versus 0.25 mg/Kg), $P=0.0056$ (vehicle versus 1.0 mg/Kg), $P=0.0121$ (vehicle versus 2.5 mg/Kg)).

(m) Scatter plot depicting the maximal ΔF/F $GRAB^{DA}$ response to food following pre-stimulation of VTA DA neurons and the associated amount of food intake following pre-stimulation of VTA DA neurons (n=8 per group, Pearson correlation, $P<0.01$). Solid line shows the linear trend line fit to the data.

(n-p) Images of hM4D(Gi) expression (red) in TH^+, VTA neurons (green) of a *DAT*::Cre mouse (n). Higher magnification of white box (o-p). Scale bar, 500 μm (n), 50 μm (p).

(q) Neurons transduced with hM4D(Gi) in the VTA and SNC (n=3, 1047, 2745, 2710 neurons each mouse, unpaired t-test, $P=0.02$).

(r) Average ΔF/F of DA signals in aDCN-LAT hM3D(Gq) mice and aDCN-LAT hM3D(Gq); VTA hM4D(Gi) mice (n=6 per group, unpaired t-test, $P=0.003$).

(g) Distance travelled by aDCN-LAT hM3D(Gq) mice and aDCN-LAT hM3D(Gq); VTA hM4D(Gi) mice during a 10-min open field session (n=6 and 7, respectively, unpaired t-test, $P=0.382$).

Data are expressed as mean ± SEM, two-sided *P* values, t-tests and post-hoc comparisons: **P*<0.05, ***P*<0.01, ****P*<0.001; ANOVA interaction: ∞∞∞∞*P*<0.001; ANOVA main effect of group: ¤¤¤*P*<0.001. SNC, substantia nigra pars compacta; TH, tyrosine hydroxylase; VTA, ventral tegmental area. Statistical analysis in Supplementary Table 1.

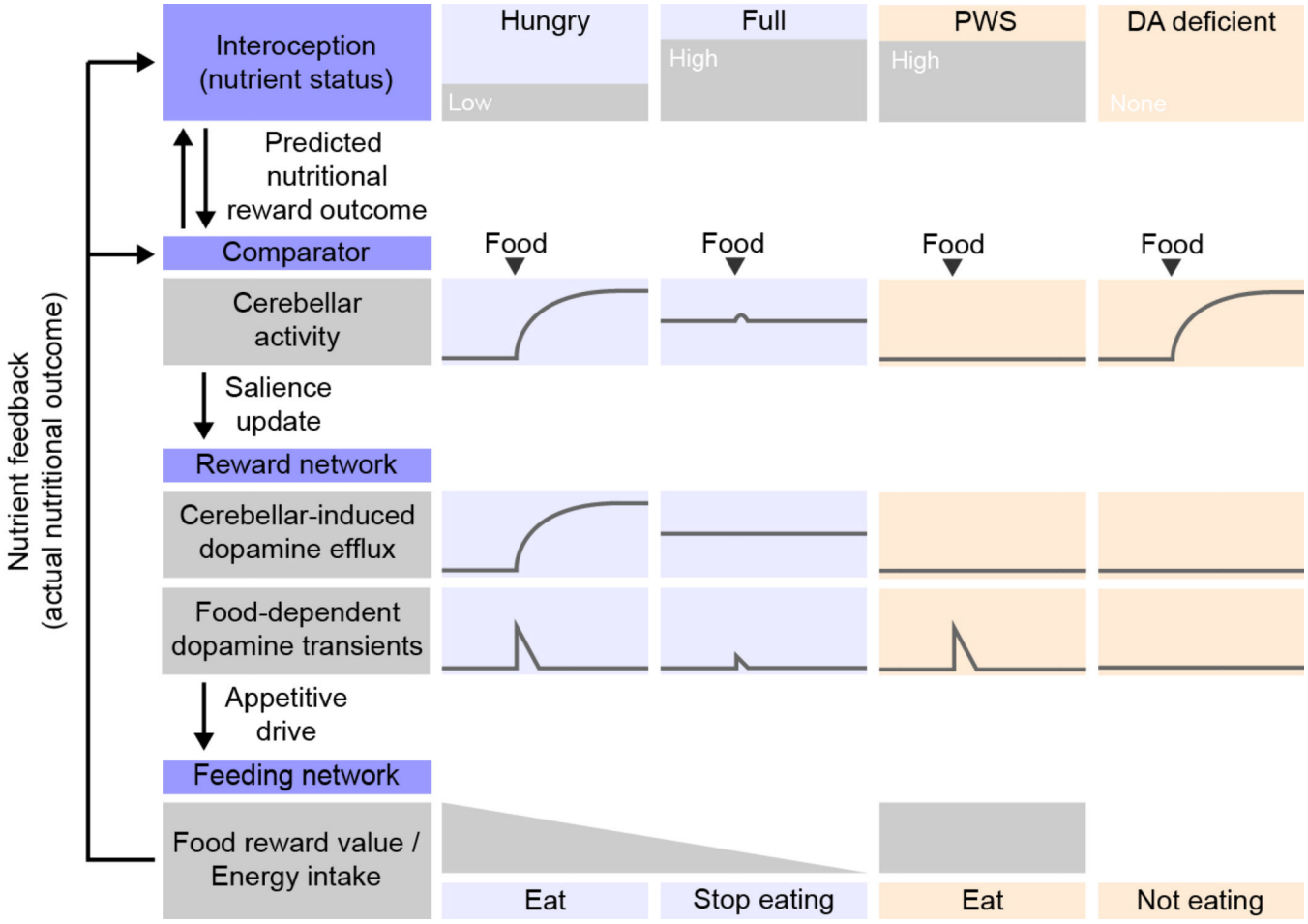

Extended Data Fig. 13 |. Proposed role of the cerebellum in feeding control

The cerebellum is well-positioned to integrate homeostatic satiation signals and is capable of orchestrating adaptive feeding responses by modulating motor, cognitive, affective and endocrine functions[20,64–73]. Visual, gustatory and olfactory inputs are all known to activate the cerebellum[74–76] which could provide salience update to control appetitive drive. It functions as a comparator of physiological nutrient state (interoception) and post-ingestion nutritional outcome (nutrient feedback) to fine-tune predictive reward signals (reward network)[77] and ultimately influence meal size (feeding network). While cerebellar output has been shown to influence VTA neuron activity[12,78], our observed changes in DA signalling are tightly associated with decreases in food intake, suggesting a dedicated role of the cerebellum in regulating DA circuits that influence feeding that is distinct from motor[78] or social[12] behaviours. Based on our mechanistic studies into the changes in the reward system mediated by the cerebellum, it is possible that previously discovered differences between PWS and control subjects arise because of cerebellar alterations[8,79,80].

In response to a predicted meal size (predicted nutritional reward outcome) by either food cues or food, cerebellar activity increases dopamine efflux that blunts dopamine transients. Consequently, the reward value of consuming food reduces and meals are terminated. In PWS patients[8,79,80], food-dependent cerebellar activity is absent and thus, dopamine transients remain regardless of amount of food consumed, leading to excessive eating. Conversely, in dopamine-deficient animals, there is a complete absence of drive to eat[14]. A better understanding of the mechanisms and circuits underlying cerebellar-mediated behaviours can guide brain stimulation strategies to control food intake recently shown to have the capability of ameliorating symptoms for disorders associated with the cerebellum[81–84].

Supplementary Material

Refer to Web version on PubMed Central for supplementary material.

Acknowledgement

We thank Hirofumi Fujita, Kimberly Gallagher, and Ayesha Thanawalla for comments on the manuscript. NG is supported by the National Science Foundation Graduate Research Fellowship Program (DGE-1845298). EA is supported by the National Institutes of Health (NIH) (DP2NS105555, R01NS111479, and U19NS112959), the Searle Scholars Program, The Pew Charitable Trusts, and the McKnight Foundation. OMS is supported by the National University of Singapore. MAH is supported by the NIH (R01MH111868; R56MH125995). ROB is supported by the NIH (R01MH116170). LMH is supported by the NIH (R01DK104772). ALA is supported by the Monell Chemical Senses Center, NIH (R00DK119574), the Klingenstein-Simons Fellowship Award, the American Heart Association (857082) and the Penn Institute for Diabetes, Obesity, and Metabolism. JNB is supported by the University of Pennsylvania School of Arts and Sciences, the American Diabetes Association (118IBS116), the American Heart Association (AHA 17SDG33400158), the Whitehall Foundation, the Klingenstein-Simons Fellowship Award and the NIH (1R01DK114104). AIC and AYTL were supported by the Warwick-NTU Neuroscience Programme. AIC, OMS and THC are supported by the Singapore Ministry of Education (MOE2018-T2-1-065). AIC and THC are supported by the Singapore Ministry of Education (MOE2017-T3-1-002). JNB and AIC are supported by the NIH (1R01DK124801).

References

1. Berthoud HR & Morrison C. The brain, appetite, and obesity. Annu Rev Psychol 59, 55–92, doi:10.1146/annurev.psych.59.103006.093551 (2008). [PubMed: 18154499]
2. Speakman JR A nonadaptive scenario explaining the genetic predisposition to obesity: the “predation release” hypothesis. Cell Metab 6, 5–12, doi:10.1016/j.cmet.2007.06.004 (2007). [PubMed: 17618852]
3. Rossi MA & Stuber GD Overlapping Brain Circuits for Homeostatic and Hedonic Feeding. Cell Metab 27, 42–56, doi:10.1016/j.cmet.2017.09.021 (2018). [PubMed: 29107504]
4. Woods SC & Ramsay DS Food intake, metabolism and homeostasis. Physiol Behav 104, 4–7, doi:10.1016/j.physbeh.2011.04.026 (2011). [PubMed: 21530564]
5. Berthoud HR The neurobiology of food intake in an obesogenic environment. Proc Nutr Soc 71, 478–487, doi:10.1017/S0029665112000602 (2012). [PubMed: 22800810]
6. Gautron L, Elmquist JK & Williams KW Neural control of energy balance: translating circuits to therapies. Cell 161, 133–145, doi:10.1016/j.cell.2015.02.023 (2015). [PubMed: 25815991]
7. Angulo MA, Butler MG & Cataletto ME Prader-Willi syndrome: a review of clinical, genetic, and endocrine findings. J Endocrinol Invest 38, 1249–1263, doi:10.1007/s40618-015-0312-9 (2015). [PubMed: 26062517]
8. Holsen LM et al. Importance of reward and prefrontal circuitry in hunger and satiety: Prader-Willi syndrome vs simple obesity. Int J Obes (Lond) 36, 638–647, doi:10.1038/ijo.2011.204 (2012). [PubMed: 22024642]

9. Barrachina MD, Martinez V, Wang L, Wei JY & Tache Y. Synergistic interaction between leptin and cholecystokinin to reduce short-term food intake in lean mice. Proc Natl Acad Sci U S A 94, 10455–10460, doi:10.1073/pnas.94.19.10455 (1997). [PubMed: 9294232]
10. Kebschull JM et al. Cerebellar nuclei evolved by repeatedly duplicating a conserved cell-type set. Science 370, doi:10.1126/science.abd5059 (2020).
11. Betley JN, Cao ZF, Ritola KD & Sternson SM Parallel, redundant circuit organization for homeostatic control of feeding behavior. Cell 155, 1337–1350, doi:10.1016/j.cell.2013.11.002 (2013). [PubMed: 24315102]
12. Carta I, Chen CH, Schott AL, Dorizan S. & Khodakhah K. Cerebellar modulation of the reward circuitry and social behavior. Science 363, doi:10.1126/science.aav0581 (2019).
13. Salamone JD, Correa M, Mingote S. & Weber SM Nucleus accumbens dopamine and the regulation of effort in food-seeking behavior: implications for studies of natural motivation, psychiatry, and drug abuse. J Pharmacol Exp Ther 305, 1–8, doi:10.1124/jpet.102.035063 (2003). [PubMed: 12649346]
14. Palmiter RD Is dopamine a physiologically relevant mediator of feeding behavior? Trends Neurosci 30, 375–381, doi:10.1016/j.tins.2007.06.004 (2007). [PubMed: 17604133]
15. Hinton EC et al. Neural representations of hunger and satiety in Prader-Willi syndrome. Int J Obes (Lond) 30, 313–321, doi:10.1038/sj.ijo.0803128 (2006). [PubMed: 16276365]
16. Chen Y, Lin YC, Kuo TW & Knight ZA Sensory detection of food rapidly modulates arcuate feeding circuits. Cell 160, 829–841, doi:10.1016/j.cell.2015.01.033 (2015). [PubMed: 25703096]
17. Betley JN et al. Neurons for hunger and thirst transmit a negative-valence teaching signal. Nature 521, 180–185, doi:10.1038/nature14416 (2015). [PubMed: 25915020]
18. Alhadeff AL et al. Natural and Drug Rewards Engage Distinct Pathways that Converge on Coordinated Hypothalamic and Reward Circuits. Neuron 103, 891–908 e896, doi:10.1016/j.neuron.2019.05.050 (2019). [PubMed: 31277924]
19. Somana R. & Walberg F. Cerebellar afferents from the nucleus of the solitary tract. Neurosci Lett 11, 41–47, doi:10.1016/0304-3940(79)90053-3 (1979). [PubMed: 431884]
20. Zhu JN & Wang JJ The cerebellum in feeding control: possible function and mechanism. Cell Mol Neurobiol 28, 469–478, doi:10.1007/s10571-007-9236-z (2008). [PubMed: 18027085]
21. Sodersten P, Bergh C, Leon M. & Zandian M. Dopamine and anorexia nervosa. Neurosci Biobehav Rev 60, 26–30, doi:10.1016/j.neubiorev.2015.11.003 (2016). [PubMed: 26608248]
22. Daberkow DP et al. Amphetamine paradoxically augments exocytotic dopamine release and phasic dopamine signals. J Neurosci 33, 452–463, doi:10.1523/JNEUROSCI.2136-12.2013 (2013). [PubMed: 23303926]
23. Alhadeff AL, Rupprecht LE & Hayes MR GLP-1 neurons in the nucleus of the solitary tract project directly to the ventral tegmental area and nucleus accumbens to control for food intake. Endocrinology 153, 647–658, doi:10.1210/en.2011-1443 (2012). [PubMed: 22128031]
24. Keiflin R, Pribut HJ, Shah NB & Janak PH Ventral Tegmental Dopamine Neurons Participate in Reward Identity Predictions. Curr Biol 29, 93–103 e103, doi:10.1016/j.cub.2018.11.050 (2019). [PubMed: 30581025]
25. Butler MG, Bittel DC, Kibiryeva N, Talebizadeh Z. & Thompson T. Behavioral differences among subjects with Prader-Willi syndrome and type I or type II deletion and maternal disomy. Pediatrics 113, 565–573 (2004). [PubMed: 14993551]
26. Holsen LM et al. Neural mechanisms underlying food motivation in children and adolescents. Neuroimage 27, 669–676, doi:10.1016/j.neuroimage.2005.04.043 (2005). [PubMed: 15993629]
27. Holsen LM et al. Neural mechanisms underlying hyperphagia in Prader-Willi syndrome. Obesity (Silver Spring) 14, 1028–1037, doi:10.1038/oby.2006.118 (2006). [PubMed: 16861608]
28. Holsen LM et al. Genetic subtype differences in neural circuitry of food motivation in Prader-Willi syndrome. Int J Obes (Lond) 33, 273–283, doi:10.1038/ijo.2008.255 (2009). [PubMed: 19048015]
29. LaBar KS et al. Hunger selectively modulates corticolimbic activation to food stimuli in humans. Behav Neurosci 115, 493–500 (2001). [PubMed: 11345973]
30. Gelman N. et al. MR imaging of human brain at 3.0 T: preliminary report on transverse relaxation rates and relation to estimated iron content. Radiology 210, 759–767 (1999). [PubMed: 10207479]

31. Whitfield-Gabrieli S. Region of interest extraction (REX) toolbox (Boston, MA). p497 (2009).
32. Vong L. et al. Leptin action on GABAergic neurons prevents obesity and reduces inhibitory tone to POMC neurons. Neuron 71, 142–154, doi:10.1016/j.neuron.2011.05.028 (2011). [PubMed: 21745644]
33. Backman CM et al. Characterization of a mouse strain expressing Cre recombinase from the 3' untranslated region of the dopamine transporter locus. Genesis 44, 383–390, doi:10.1002/dvg.20228 (2006). [PubMed: 16865686]
34. Allen WE et al. Thirst-associated preoptic neurons encode an aversive motivational drive. Science 357, 1149–1155, doi:10.1126/science.aan6747 (2017). [PubMed: 28912243]
35. Madisen L. et al. A toolbox of Cre-dependent optogenetic transgenic mice for light-induced activation and silencing. Nat Neurosci 15, 793–802, doi:10.1038/nn.3078 (2012). [PubMed: 22446880]
36. Borgius L, Restrepo CE, Leao RN, Saleh N. & Kiehn O. A transgenic mouse line for molecular genetic analysis of excitatory glutamatergic neurons. Mol Cell Neurosci 45, 245–257, doi:10.1016/j.mcn.2010.06.016 (2010). [PubMed: 20600924]
37. Tong Q, Ye CP, Jones JE, Elmquist JK & Lowell BB Synaptic release of GABA by AgRP neurons is required for normal regulation of energy balance. Nat Neurosci 11, 998–1000, doi:10.1038/nn.2167 (2008). [PubMed: 19160495]
38. Su Z, Alhadeff AL & Betley JN Nutritive, Post-ingestive Signals Are the Primary Regulators of AgRP Neuron Activity. Cell Rep 21, 2724–2736, doi:10.1016/j.celrep.2017.11.036 (2017). [PubMed: 29212021]
39. Alhadeff AL, Park O, Hernandez E. & Betley JN Inhibition of Itch by Hunger and AgRP Neuron Activity. Neuroscience, doi:10.1016/j.neuroscience.2020.06.005 (2020).
40. Sun F. et al. A Genetically Encoded Fluorescent Sensor Enables Rapid and Specific Detection of Dopamine in Flies, Fish, and Mice. Cell 174, 481–496 e419, doi:10.1016/j.cell.2018.06.042 (2018). [PubMed: 30007419]
41. Goebel M, Stengel A, Wang L. & Tache Y. Central nesfatin-1 reduces the nocturnal food intake in mice by reducing meal size and increasing inter-meal intervals. Peptides 32, 36–43, doi:10.1016/j.peptides.2010.09.027 (2011). [PubMed: 20933030]
42. Lerner TN et al. Intact-Brain Analyses Reveal Distinct Information Carried by SNc Dopamine Subcircuits. Cell 162, 635–647, doi:10.1016/j.cell.2015.07.014 (2015). [PubMed: 26232229]
43. Zalocusky KA et al. Nucleus accumbens D2R cells signal prior outcomes and control risky decision-making. Nature 531, 642–646, doi:10.1038/nature17400 (2016). [PubMed: 27007845]
44. Weir JB New methods for calculating metabolic rate with special reference to protein metabolism. 1949. Nutrition 6, 213–221 (1990). [PubMed: 2136000]
45. Betley JN et al. Stringent specificity in the construction of a GABAergic presynaptic inhibitory circuit. Cell 139, 161–174, doi:10.1016/j.cell.2009.08.027 (2009). [PubMed: 19804761]
46. Young MD & Behjati S. SoupX removes ambient RNA contamination from droplet based single-cell RNA sequencing data. bioRxiv (2020).
47. Stuart T. et al. Comprehensive Integration of Single-Cell Data. Cell 177, 1888–1902 e1821, doi:10.1016/j.cell.2019.05.031 (2019). [PubMed: 31178118]
48. Wolf FA, Angerer P. & Theis FJ SCANPY: large-scale single-cell gene expression data analysis. Genome Biol 19, 15, doi:10.1186/s13059-017-1382-0 (2018). [PubMed: 29409532]
49. Levine JH et al. Data-Driven Phenotypic Dissection of AML Reveals Progenitor-like Cells that Correlate with Prognosis. Cell 162, 184–197, doi:10.1016/j.cell.2015.05.047 (2015). [PubMed: 26095251]
50. McGinnis CS, Murrow LM & Gartner ZJ DoubletFinder: Doublet Detection in Single-Cell RNA Sequencing Data Using Artificial Nearest Neighbors. Cell Syst 8, 329–337 e324, doi:10.1016/j.cels.2019.03.003 (2019). [PubMed: 30954475]
51. Hafemeister C. & Satija R. Normalization and variance stabilization of single-cell RNA-seq data using regularized negative binomial regression. Genome Biol 20, 296, doi:10.1186/s13059-019-1874-1 (2019). [PubMed: 31870423]
52. Becht E. et al. Dimensionality reduction for visualizing single-cell data using UMAP. Nat Biotechnol, doi:10.1038/nbt.4314 (2018).

53. Marques S. et al. Oligodendrocyte heterogeneity in the mouse juvenile and adult central nervous system. Science 352, 1326–1329, doi:10.1126/science.aaf6463 (2016). [PubMed: 27284195]
54. Saunders A. et al. Molecular Diversity and Specializations among the Cells of the Adult Mouse Brain. Cell 174, 1015–1030 e1016, doi:10.1016/j.cell.2018.07.028 (2018). [PubMed: 30096299]
55. Vanlandewijck M. et al. A molecular atlas of cell types and zonation in the brain vasculature. Nature 554, 475–480, doi:10.1038/nature25739 (2018). [PubMed: 29443965]
56. Zeisel A. et al. Molecular Architecture of the Mouse Nervous System. Cell 174, 999–1014 e1022, doi:10.1016/j.cell.2018.06.021 (2018). [PubMed: 30096314]
57. Carter RA et al. A Single-Cell Transcriptional Atlas of the Developing Murine Cerebellum. Curr Biol 28, 2910–2920 e2912, doi:10.1016/j.cub.2018.07.062 (2018). [PubMed: 30220501]
58. Wizeman JW, Guo Q, Wilion EM & Li JY Specification of diverse cell types during early neurogenesis of the mouse cerebellum. Elife 8, doi:10.7554/eLife.42388 (2019).
59. Goldstein N. et al. Hypothalamic detection of macronutrients via multiple gut-brain pathways. Cell Metab, doi:10.1016/j.cmet.2020.12.018 (2021).
60. Andermann ML & Lowell BB Toward a Wiring Diagram Understanding of Appetite Control. Neuron 95, 757–778, doi:10.1016/j.neuron.2017.06.014 (2017). [PubMed: 28817798]
61. Brakeman PR et al. Homer: a protein that selectively binds metabotropic glutamate receptors. Nature 386, 284–288, doi:10.1038/386284a0 (1997). [PubMed: 9069287]
62. Berridge KC 'Liking' and 'wanting' food rewards: brain substrates and roles in eating disorders. Physiol Behav 97, 537–550, doi:10.1016/j.physbeh.2009.02.044 (2009). [PubMed: 19336238]
63. Wise RA Role of brain dopamine in food reward and reinforcement. Philosophical transactions of the Royal Society of London. Series B, Biological sciences 361, 1149–1158, doi:10.1098/rstb.2006.1854 (2006). [PubMed: 16874930]
64. Becker MI & Person AL Cerebellar Control of Reach Kinematics for Endpoint Precision. Neuron 103, 335–348 e335, doi:10.1016/j.neuron.2019.05.007 (2019). [PubMed: 31174960]
65. Dacre J. et al. A cerebellar-thalamocortical pathway drives behavioral context-dependent movement initiation. Neuron 109, 2326–2338 e2328, doi:10.1016/j.neuron.2021.05.016 (2021). [PubMed: 34146469]
66. Darmohray DM, Jacobs JR, Marques HG & Carey MR Spatial and Temporal Locomotor Learning in Mouse Cerebellum. Neuron 102, 217–231 e214, doi:10.1016/j.neuron.2019.01.038 (2019). [PubMed: 30795901]
67. Frontera JL et al. Bidirectional control of fear memories by cerebellar neurons projecting to the ventrolateral periaqueductal grey. Nat Commun 11, 5207, doi:10.1038/s41467-020-18953-0 (2020). [PubMed: 33060630]
68. Gao Z. et al. A cortico-cerebellar loop for motor planning. Nature 563, 113–116, doi:10.1038/s41586-018-0633-x (2018). [PubMed: 30333626]
69. Kelly E. et al. Regulation of autism-relevant behaviors by cerebellar-prefrontal cortical circuits. Nat Neurosci 23, 1102–1110, doi:10.1038/s41593-020-0665-z (2020). [PubMed: 32661395]
70. Xiao L, Bornmann C, Hatstatt-Burkle L. & Scheiffele P. Regulation of striatal cells and goal-directed behavior by cerebellar outputs. Nat Commun 9, 3133, doi:10.1038/s41467-018-05565-y (2018). [PubMed: 30087345]
71. Giovannucci A. et al. Cerebellar granule cells acquire a widespread predictive feedback signal during motor learning. Nat Neurosci 20, 727–734, doi:10.1038/nn.4531 (2017). [PubMed: 28319608]
72. Locke TM et al. Dopamine D1 Receptor-Positive Neurons in the Lateral Nucleus of the Cerebellum Contribute to Cognitive Behavior. Biol Psychiatry 84, 401–412, doi:10.1016/j.biopsych.2018.01.019 (2018). [PubMed: 29478701]
73. Fujita H, Kodama T. & du Lac S. Modular output circuits of the fastigial nucleus mediate diverse motor and nonmotor functions of the cerebellar vermis. eLife e58613, doi:10.1101/2020.04.23.047100 (2020).
74. DiFeliceantonio AG et al. Supra-Additive Effects of Combining Fat and Carbohydrate on Food Reward. Cell Metab 28, 33–44 e33, doi:10.1016/j.cmet.2018.05.018 (2018). [PubMed: 29909968]

75. Kralj-Hans I, Baizer JS, Swales C. & Glickstein M. Independent roles for the dorsal paraflocculus and vermal lobule VII of the cerebellum in visuomotor coordination. Exp Brain Res 177, 209–222, doi:10.1007/s00221-006-0661-x (2007). [PubMed: 16951960]

76. Sobel N. et al. Odorant-induced and sniff-induced activation in the cerebellum of the human. J Neurosci 18, 8990–9001 (1998). [PubMed: 9787004]

77. Wagner MJ, Kim TH, Savall J, Schnitzer MJ & Luo L. Cerebellar granule cells encode the expectation of reward. Nature 544, 96–100, doi:10.1038/nature21726 (2017). [PubMed: 28321129]

78. Nieoullon A, Cheramy A. & Glowinski J. Release of dopamine in both caudate nuclei and both substantia nigrae in response to unilateral stimulation of cerebellar nuclei in the cat. Brain Res 148, 143–152, doi:10.1016/0006-8993(78)90384-0 (1978). [PubMed: 656921]

79. Miller JL et al. Enhanced activation of reward mediating prefrontal regions in response to food stimuli in Prader-Willi syndrome. J Neurol Neurosurg Psychiatry 78, 615–619, doi:10.1136/jnnp.2006.099044 (2007). [PubMed: 17158560]

80. Shapira NA et al. Satiety dysfunction in Prader-Willi syndrome demonstrated by fMRI. J Neurol Neurosurg Psychiatry 76, 260–262, doi:10.1136/jnnp.2004.039024 (2005). [PubMed: 15654046]

81. Brady RO Jr. et al. Cerebellar-Prefrontal Network Connectivity and Negative Symptoms in Schizophrenia. Am J Psychiatry 176, 512–520, doi:10.1176/appi.ajp.2018.18040429 (2019). [PubMed: 30696271]

82. Halko MA, Farzan F, Eldaief MC, Schmahmann JD & Pascual-Leone A. Intermittent theta-burst stimulation of the lateral cerebellum increases functional connectivity of the default network. J Neurosci 34, 12049–12056, doi:10.1523/JNEUROSCI.1776-14.2014 (2014). [PubMed: 25186750]

83. Miterko LN et al. Neuromodulation of the cerebellum rescues movement in a mouse model of ataxia. Nat Commun 12, 1295, doi:10.1038/s41467-021-21417-8 (2021). [PubMed: 33637754]

84. Stoodley CJ et al. Altered cerebellar connectivity in autism and cerebellar-mediated rescue of autism-related behaviors in mice. Nat Neurosci 20, 1744–1751, doi:10.1038/s41593-017-0004-1 (2017). [PubMed: 29184200]

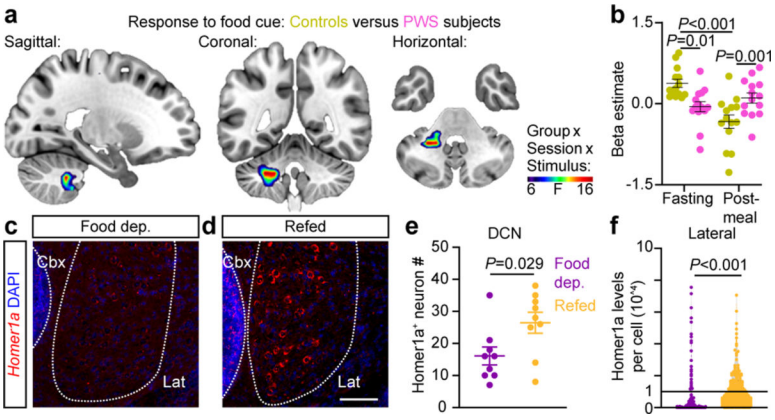

Fig. 1 |. The deep cerebellum is activated by food

(a) Hunger state-dependent responses to food cues in brains of subjects with Prader-Willi syndrome (PWS) and controls, centred on the peak voxel of activation (MNI coordinates: −24, −49, −38) exceeding a significance threshold of P<0.01, uncorrected, and an extent threshold of k=50 (n=14/group).

(b) Post-hoc analysis of signal change (beta estimates from the cerebellar cluster in a) in response to food vs. non-food cues in the fasting and post-meal groups of hyperphagia and control subjects (n=14/group, full factorial ANOVA).

(c, d) *Homer1a* expression (red) and DAPI (blue) in the lateral nucleus of the DCN of food-deprived (c) and refed (d) mice. Scale bar, 100 μm.

(e) Number of *Homer1a*$^{+}$ DCN neurons (n=3/group, unpaired t-test).

(f) *Homer1a* expression level in individual lateral nucleus neurons (n=3/group, unpaired t-test).

Data expressed as mean±SEM, and two-sided P values. Cbx, cerebellar cortex; Lat, lateral nucleus. Statistical analysis in Supplementary Table 1.

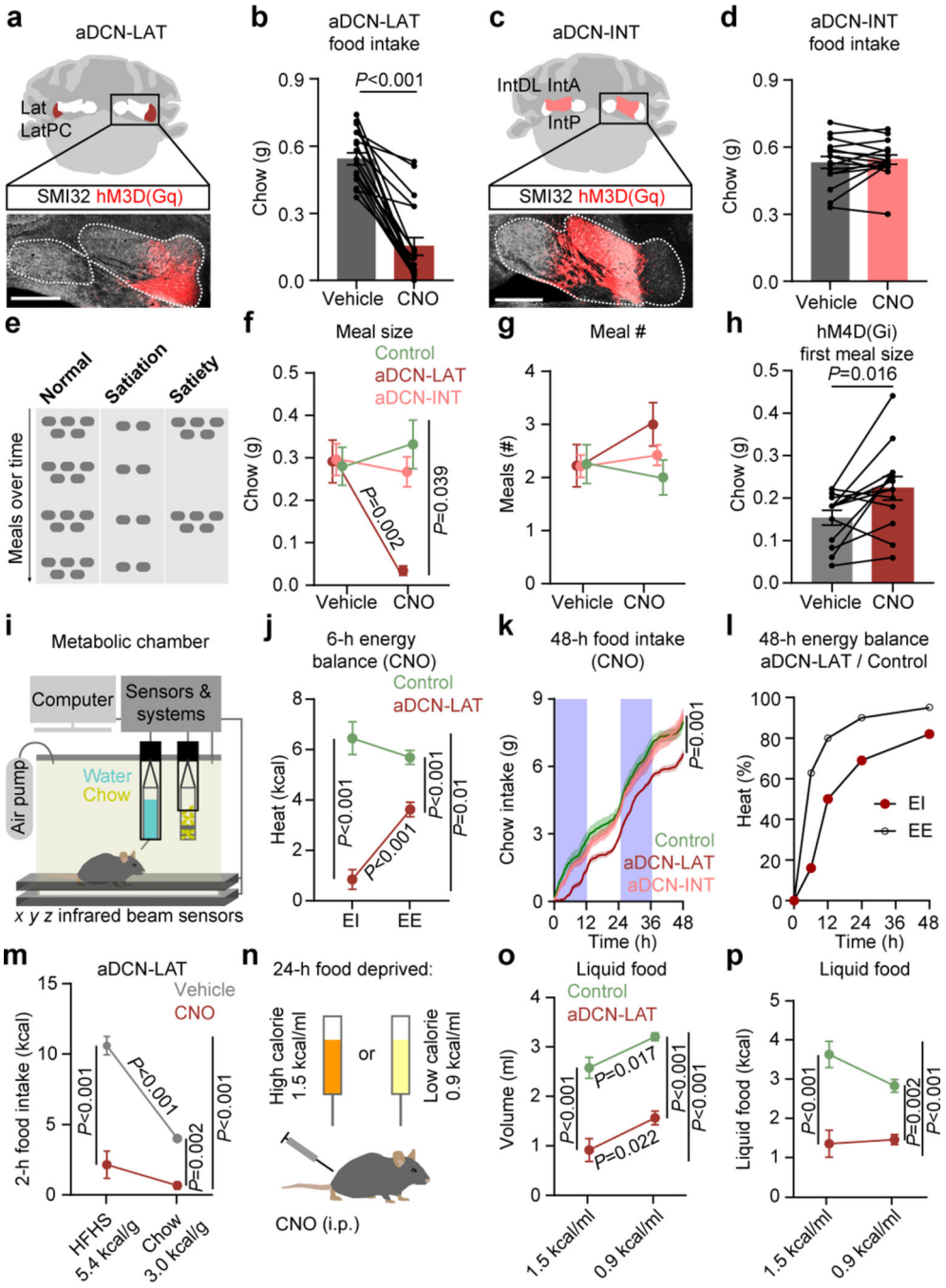

Fig. 2 |. Activation of aDCN suppresses food intake without metabolic compensation

(a) hM3D(Gq) expression in aDCN-LAT (grey: SMI32, red: hM3D(Gq)). Scale bar, 500 μm.

(b) 1-h food intake in food-deprived mice with aDCN-LAT activation (n=19, paired t-test).

(c) hM3D(Gq) expression in aDCN-INT (grey: SMI32, red: hM3D(Gq)). Scale bar, 500 μm.

(d) 1-h food intake in food-deprived mice with aDCN-INT activation (n=16, paired t-test).

(e) Satiation (meal size) and satiety (inter-meal interval) as mechanisms of food intake reduction.

(f) Meal size following 24-h food deprivation (mCherry: n=8, aDCN-LAT; hM3D(Gq): n=9, aDCN-INT; hM3D(Gq): n=16, two-way ANOVA, Holm-Sidak's).
(g) Number of meals consumed during 1-h chow intake following 24-h food deprivation (mCherry: n=8, aDCN-LAT: n=9, aDCN-INT: n=16, two-way ANOVA, Holm-Sidak's).
(h) First meal size in ad libitum fed mice with aDCN-LAT inactivation (n=13, paired t-test).
(i) Metabolic monitoring schematic.
(j) Energy intake (EI) and expenditure (EE) (6-h, n=7 control, 8 aDCN-LAT activation, two-way ANOVA, Holm-Sidak's).
(k) Chow intake during 48-h period (n=8/group, two-way ANOVA, Holm-Sidak's).
(l) EI and EE during 48-h period (n=8/group).
(m) Calorie intake of chow or HFHS diet following 24-h food deprivation (n=9; repeated measures two-way ANOVA, Holm-Sidak's).
(n) Low (Ensure®, 0.9 kcal/ml) and high (Ensure PLUS®, 1.5 kcal/ml) calorie liquid meal consumption assay.
(o) Volume of intake during 1-h period (mCherry: n=13, aDCN-LAT activation: n=9, two-way ANOVA, Holm-Sidak's).
(p) Kcal consumed during 1-h period (mCherry: n=13, aDCN-LAT activation: n=9, two-way ANOVA, Holm-Sidak's).
Data expressed as mean±SEM, and two-sided P values. See Supplementary Table 1.

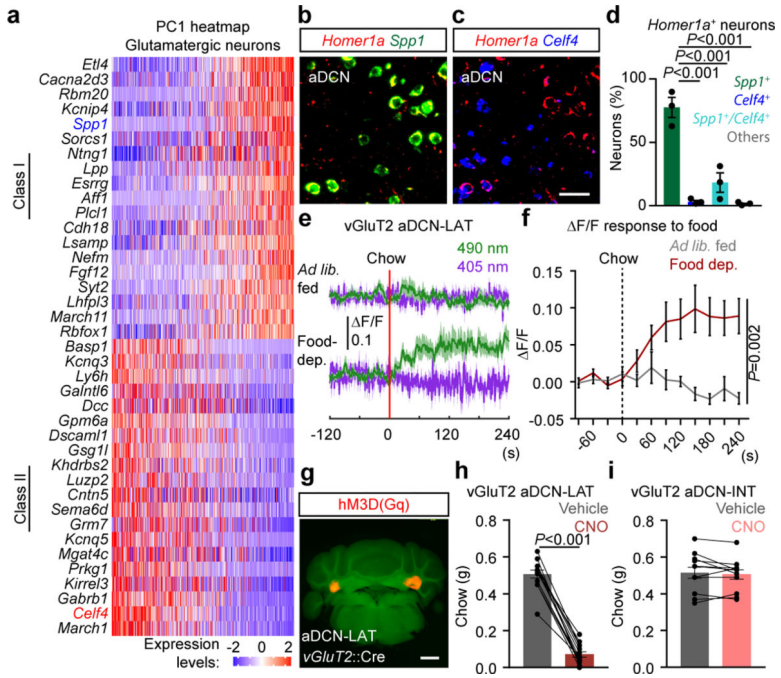

Fig. 3 |. Molecular and topographical organization of nutrient-sensing DCN neurons

(a) Expression level of transcripts in class I and II glutamatergic DCN neurons.

(b-c) *Homer1a* (red), *Spp1* (green) and *Celf4* (blue) expression in the aDCN. Scale bar, 50 μm.

(d) Quantification of *Homer1a*$^{+}$ neurons in the aDCN of food-deprived mice after refeeding (n=3, one-way ANOVA, Holm-Sidak's).

(e) Average GCaMP6 signal in aDCN-LAT neurons of ad libitum fed (top) or food-deprived (bottom) mice (490 nm, green, control 405 nm, magenta). Signals are aligned to the introduction of chow (red line). Dark line represents the mean and lighter shaded area represents SEMs (n=7).

(f) Average GCaMP6s signal in 30-s bins of aDCN-LAT neurons in ad libitum fed (grey) or food-deprived (red) mice in response to chow (dotted line) (n=7, repeated measures two-way ANOVA).

(g) Expression of hM3D(Gq) (red) in aDCN-LAT neurons of vGluT2::Cre mouse. Scale bar, 1000 μm.

(h) Chow intake in food-deprived mice with aDCN-LAT vGluT2 neuron activation (n=14, paired t-test).

(i) Chow intake in food-deprived mice with aDCN-INT vGluT2 neuron activation (n=12, paired t-test).

Data expressed as mean±SEM, two-sided P values. See Supplementary Table 1.

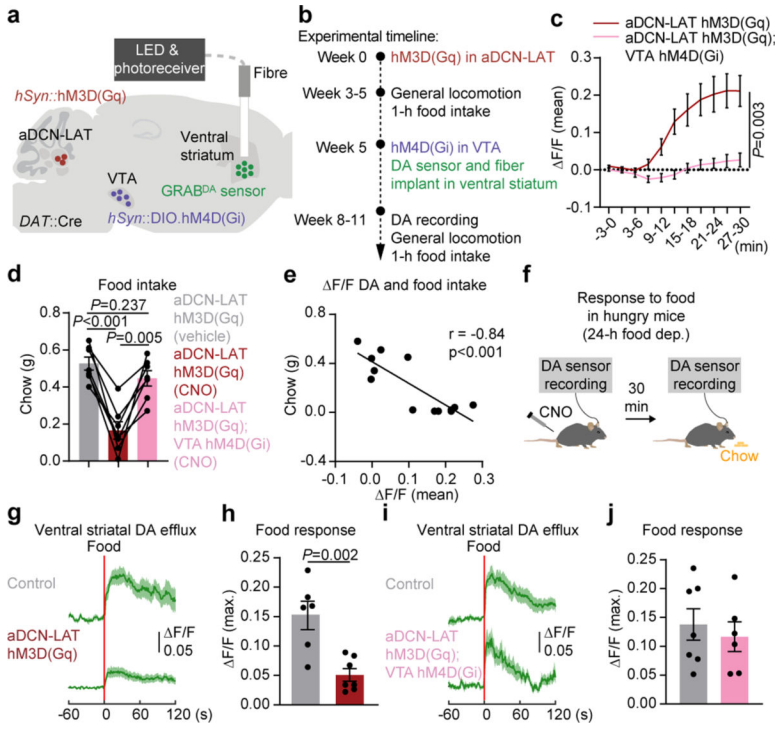

Fig. 4 |. aDCN suppresses food intake via hedonic, but not homeostatic, signaling

(a) Schematic depicting experimental paradigm: hM3D(Gq) in the aDCN and hM4D(Gi) in VTA-DA neurons, and GRAB^{DA} and fibre in the ventral striatum of a *DAT*::Cre mouse.

(b) Experimental timeline.

(c) Average GRABDA signal in 3-min bins (n=6/group, repeated measures two-way ANOVA).

(d) Food intake in mice with aDCN-LAT activation alone or mice with aDCN-LAT activation and VTA-DA neuron inhibition (n=7, repeated measures one-way ANOVA, Holm-Sidak's).

(e) Food intake and average GRABDA signal (n=13, respectively, Pearson correlation).

(f) Fibre photometry recording of GRABDA to food presentation in CNO-treated, food-deprived mice.

(g) GRABDA signals in the ventral striatum. Signals are aligned to the food presentation (red line). Dark line represents mean and lighter shaded area represents SEMs (n=6 control, 7 aDCN-LAT-hM3D(Gq)).

(h) Maximum DA signal (n=6 control, 7 aDCN-LAT-hM3D(Gq), unpaired t-test).

(i) Average GRABDA signal in the ventral striatum. Signals are aligned to the food presentation (red line). Dark line represents the mean and lighter shaded area represents SEMs (n=7 control, n=6 aDCN-LAT hM3D(Gq); VTA hM4D(Gi)).

(j) Maximum DA signal (n=7 control, n=6 aDCN-LAT hM3D(Gq); VTA hM4D(Gi), unpaired t-test).

Data are expressed as mean±SEM, two-sided P values. ARC, arcuate nucleus; VTA, ventral tegmental area. See Supplementary Table 1.